

Nuclear Stellar Populations in the Infrared Space Observatory Atlas of Bright Spiral Galaxies

George J. Bendo,^{1,2,3} Robert D. Joseph,^{2,4}

ABSTRACT

To understand the nuclear stellar populations and star formation histories of the nuclei of spiral galaxies, we have obtained K-band nuclear spectra for 41 galaxies and H-band spectra for 20 galaxies in the ISO Atlas of Bright Spiral Galaxies. In the vast majority of the subsample (80%), the near-infrared spectra suggest that evolved red stars completely dominate the nuclear stellar populations and that hot young stars are virtually non-existent. The signatures of recent star formation activity are only found in 20% of the subsample, even though older red stars still dominate the stellar populations in these galaxies. Given the dominance of evolved stars in most galaxy nuclei and the nature of the emission lines in the galaxies where they were detected, we suggest that nuclear star formation proceeds in the form of instantaneous bursts. The stars produced by these bursts comprise only $\sim 2\%$ of the total nuclear stellar mass in these galaxies, but we demonstrate how the nuclear stellar populations of normal spiral galaxies can be built up through a series of these bursts. The bursts were detected only in Sbc galaxies and later, and both bars and interactions appeared to be sufficient but not necessary triggers for the nuclear star formation activity. The vast majority of galaxies with nuclear star formation were classified as HII galaxies. With one exception, LINERs and transition objects were dominated by older red stars, which suggested that star formation was not responsible for generating these galaxies' optical line emission.

Subject headings: galaxies: stellar content — galaxies: nuclei

1. Introduction

The nuclear stellar populations of galaxies can reveal important information on the history of nuclear star formation, which could then reveal the mechanisms behind triggering star formation.

¹Steward Observatory, 933 North Cherry Avenue, Tucson, AZ 85721, USA; gbendo@as.arizona.edu

²Visiting Astronomer at the Infrared Telescope Facility, which is operated by the University of Hawaii under contract from the National Aeronautics and Space Administration.

³Visiting Astronomer at the UH 2.2 m Telescope at Mauna Kea Observatory, Institute for Astronomy, University of Hawaii.

⁴University of Hawaii, Institute for Astronomy, 2680 Woodlawn Drive, Honolulu, HI 96822, USA; joseph@ifa.hawaii.edu

Understanding nuclear stellar populations is therefore important to understanding the evolution of galaxies and the enhancement of star formation in the universe. Near-infrared spectroscopy is ideal for studying stellar populations because it traces not only the presence of hot young stars through near-infrared hydrogen recombination lines, such as the Brackett γ line, but also the presence of red stars, particularly red supergiants, and the presence of shocks from supernovae activity. Red supergiants and giants can be determined from the presence of various absorption features in the H- and K-bands, such as the CO and Si I absorption features in the H-band and the CO bands longward of $2.29 \mu\text{m}$ (Origlia, Moorwood, & Oliva 1993). Supernova activity can be inferred from the presence of Fe II emission lines associated with the supernova activity (Oliva, Moorwood, & Danziger 1989; Greenhouse et al. 1991; Colina 1993; Forbes & Ward 1993; Greenhouse et al. 1997; Morel, Doyon, & St-Louis 2002; Alonso-Herrero et al. 2003) and possibly even molecular hydrogen line emission (Oliva, Moorwood, & Danziger 1989; Greenhouse et al. 1991; Forbes & Ward 1993) (although molecular hydrogen line emission may be produced by other sources; see Mouri (1994) and Vanzi & Rieke (1997)). These diagnostics can be used together to characterize the different ages of the various stellar populations within galactic nuclei.

Once the nuclear stellar populations of spiral galaxies are well defined, they can be used to answer a number of specific scientific questions. To begin with, this will illuminate how star formation proceeds in the nuclei of “normal” spiral galaxies, and whether that star formation is either continuous or a series of short bursts. Once we understand the functionality of star formation over time, we can determine how the nuclei of spiral galaxies have evolved. We can also determine how morphological features, particularly bars, or how environmental influences, such as interactions, influence nuclear star formation activity. Additionally, we can probe the link between star formation activity and Seyfert or LINER activity.

Much of the work at near-infrared wavelengths has focused on unusual objects with either AGN or very strong star formation activity. Recent surveys include surveys of ultraluminous infrared galaxies (Goldader et al. 1995; Murphy et al. 1999, 2001; Burston, Ward, & Davies 2001), luminous infrared galaxies (Goldader et al. 1997), starbursts (Engelbracht 1997; Ivanov 2000; Coziol, Doyon, & Demers 2001), Seyferts (Ivanov 2000; Sosa-Brito, Tacconi-Garman, & Lehnert 2001; Reunanen, Kotilainen, & Prieto 2002; Boisson et al. 2002), LINERs (Larkin et al. 1998; Alonso-Herrero et al. 2000; Sosa-Brito, Tacconi-Garman, & Lehnert 2001), and interacting galaxies (Vanzi, Alonso-Herrero, & Rieke 1998). However, relatively little near-infrared spectroscopic survey has been done with “normal” nearby spiral galaxies (see Mannucci et al. (2001) for an example). Such surveys are necessary, though, for understanding nuclear star formation histories, for identifying the triggers that enhance nuclear star formation, and for setting a baseline for the H- and K-band emission from normal spiral galaxies. Without such a baseline, the contribution of relatively quiescent stellar populations to H- and K-band emission in starbursts as well as the older stars’ contribution to the overall mass and luminosities in these systems will remain unknown, and the enhancement in star formation activity in exotic systems like ultraluminous infrared galaxies will have no context.

Therefore, we have undertaken a near-infrared spectroscopic survey of a subset of the galaxies

in the ISO Atlas of Bright Spiral Galaxies (Bendo et al. (2002a), henceforth referred to as Paper 1) with the purpose of understanding the nuclear stellar populations and star formation histories of these objects. The data includes K-band spectroscopy for 41 galaxies, with additional H-band spectroscopy for 20 galaxies. We first discuss in Section 2 the sample, the observations, and the data processing. Next, we divide the galaxies into two groups: quiescent galaxies and non-quiescent galaxies. In Section 3, the spectra of the quiescent galaxies are described in detail, combined together to make a composite quiescent spectrum, and analyzed using population synthesis models. The non-quiescent galaxies are also described in detail in Section 4, with particular focus on how their nuclear star formation activity may be related to morphology, environment, and AGN activity. After this, we determine the relative fractions of stars formed from starbursts in these systems. Finally, in Section 5, we compare quiescent and non-quiescent galaxies in plots of the $\frac{f_{12\mu m}}{f_K}$ ratio to the $f_{12\mu m}$ or f_K luminosities for the inner $15''$ as an effort to justify using mid-infrared fluxes normalized by K-band fluxes (used in Bendo et al. (2002b), henceforth referred to as Paper 2) to trace star formation activity.

2. Data

2.1. Sample

The galaxies in this ISO Bright Galaxies Project sample are a subset of a complete, magnitude-limited set of galaxies selected from the Revised Shapley-Ames (RSA) Catalog (Sandage & Tammann 1987). The sample comprised galaxies with Hubble types between S0 and Sd and with magnitudes $B_T = 12$ or brighter; galaxies in the Virgo Cluster were excluded. A randomly selected, subset of these galaxies was observed by ISO based on target visibility. This produced a total of 77 galaxies that are representative of the range of Hubble types in the RSA Catalog. Detailed information on the sample is presented in Paper 1.

Of these 77 galaxies, we observed all targets that could be feasibly observed with the the CGS4 infrared spectrometer at the United Kingdom Infrared Telescope as well as some additional targets that were observable with the SPEX near-infrared spectrometer at the NASA Infrared Telescope Facility (Rayner et al. 2003). This presented two constraints on the subsample. The first was on the sensitivity of the instruments. We were effectively limited to working with targets where the continuum could be detected above the sky noise within 2 min because of the timescale of the variability of atmospheric emission lines that produced the background emission in our spectra. The other constraint was created by the declination range of the telescopes used. All observed targets had to fall within the declination range of $-51 < \delta < +66$. In the end, a subset of 41 galaxies in K-band and 20 galaxies in H-band were observed with one of the spectrometers with sufficient signal-to-noise in their spectra for analysis. Details on the morphology, distances, and nuclear activity of this subsample are given in Tabel 1.

2.2. Observations

Details on specific information about the observations of individual galaxies are given in Tables 2 and 3. General information on the observations with each specific instrument is given below.

2.2.1. SPEX

SPEX observations were made on UT dates 5 - 8 June 2000; 16, 17, and 19 September 2000; and 4 - 5 April 2001. Each target was observed with the instrument in the short wavelength cross-dispersed mode, which covered a wavelength range from 0.8 to 2.5 μm (although we only use the 1.2 - 2.5 μm range). The slit used was $0.5 \times 15''$, giving a spectral resolution of 1200. The galaxies' nuclei (in the J- or K-band) were centered in the slit and used for guiding in all cases. The observations consist of a series of alternating 2 min observations of the galaxies and 2 min observations of an empty region of sky $\sim 2'$ off the source, with total on-source integration times of 20 - 30 min. Argon lamp spectra were taken for wavelength calibration, and quartz tungsten halogen (QTH) lamp spectra were taken for flatfielding the spectra. An A0V star was observed as a spectroscopic standard for all targets, and, for targets observed in September 2000 and April 2001, a G type star was also observed as a spectroscopic standard. The spectroscopic standards were selected to be as close to the target galaxies as possible, preferably within 10° . These stars were observed using the same configuration and methods that the galaxies were observed with except that the integration times were shorter and that the stars observed in September 2000 and April 2001 were observed by nodding along the slit rather than completely off-source.

2.2.2. CGS4

CGS H- and K-band spectroscopic observations were made on UT dates 7 - 10 May 2001. The observations were taken with the 40 lines mm^{-1} grating, and the slit used was $0.5 \times 15''$, giving a spectral resolution of ~ 800 . The galaxies' nuclei (in H- and K-band) were centered in the slit in all cases, and off-source point sources were used for guiding. The observations consist of a series of alternating 2 min observations of the galaxies and 2 min observations of an empty region of sky $\sim 2'$ off the source, with total on-source integration times of 20 min. Bias frames were taken for removing systematic readout effects, Argon lamp spectra were taken for wavelength calibration, and incandescent lamp spectra were taken for flatfielding the spectra. For each galaxy, a G type star was observed as a spectroscopic standard. The spectroscopic standards were selected to be as close to the target galaxies as possible, preferably within 10° . These stars were observed using the same configuration and methods that the galaxies were observed with except that the integration times were shorter and that the stars were observed by nodding along the slit as opposed to completely off-source.

2.3. Data Reduction

2.3.1. SPEX

First, the background frames were subtracted from the target frames. Next, the frames were divided by the QTH lamp frames. The individual orders were extracted from each frame, and spectra of the central sources were extracted from the H and K orders. The spectra were wavelength calibrated using Argon arc lamp spectra. The slopes of the spectra were corrected to account for small changes in the waveband covered per pixel. Next, the spectra from each frame were normalized relative to each other by performing a least-squares fit to solve for the scalar multiplier that minimized the differences between the first spectrum and subsequent spectra. For each wavelength value, the data were then combined in an iterative process where data points that deviated by more than 3 standard deviations from the median were removed until all data points were within three standard deviations of the median; the median and standard deviation of the mean were then taken as the flux density measurement and the error at that wavelength. Finally, the spectra were smoothed using a Gaussian function.

The spectroscopic standard was processed the same way, except that the blackbody emission was divided out and the hydrogen recombination lines were removed using one of two possible methods. In some cases, the lines were simply removed by fitting the sums of a Voigt function and a continuum to the region with the line, then adding the Voigt function to the spectra. This was most effective for removing the Brackett- γ lines from A0V and G spectroscopic standards. Other lines were removed by dividing the spectra by the spectra of previously observed stars of the same type. This was most effective for removing higher order Brackett lines from the H-band spectra of A0V standards (using data from Meyer et al. (1998)). If both A0V and G type stars had been observed, then a spectroscopic standard spectrum was made by using the A0V spectrum but by replacing the region around the Brackett- γ line with the spectrum from the G type star. Otherwise, the full spectrum of the A0V star was used as the spectroscopic standard spectrum. Once all the spectra were ready, the galaxy spectra were then divided by their corresponding spectroscopic standard spectra.

2.3.2. CGS4

Data reduction for CGS4 data followed the data processing for SPEX data with some exceptions. First, only one linear order was present in the spectra, so no work needed to be done extracting the orders. Second, since only G type spectroscopic standards were observed, only the Brackett- γ line needed to be corrected in the K-band; the hydrogen recombination lines were so weak in the H-band spectra that no corrections needed to be made. Third, the sampling of the spectra performed during the observations produced a step pattern between odd and even pixels that needed to be removed from the individual spectroscopic standard spectra before they were

median combined.

3. Quiescent Spectra

33 of the 41 nuclear K-band spectra we examined had nearly identical spectra with identical qualitative characteristics:

- The spectra all have similar slopes, at least from 2.10 μm to the edge of the first CO band at 2.29 μm .

- The spectra all contain strong CO absorption lines that are characteristically found in K and M stars (see examples in Kleinmann & Hall (1986), Lançon & Rocca-Volmerange (1992), Origlia, Moorwood, & Oliva (1993), Wallace & Hinkle (1997), and Förster Schreiber (2000)).

- The spectra all contain various metal absorption features, most notably the Na I lines at 2.206 and 2.209 μm and the Ca I lines at 2.261, 2.263, and 2.266 μm , that are most prominent in K and M stars (see examples in Kleinmann & Hall (1986), Wallace & Hinkle (1997), and Förster Schreiber (2000)).

- No Brackett- γ emission lines are evident in the spectra. Although ionized gas may be present, the negligible recombination line flux in the K-band implies relatively few young stars and therefore relatively little recent star formation activity.

- No H₂ lines are evident in the spectra. If H₂ line emission is interpreted as originating from shocks connected to supernova activity, then the lack of these lines in the spectra of these galaxies implies that nuclear supernova activity is relatively weak or nonexistent.

The H-band spectra for 15 of these 33 “quiescent” spectra share similar characteristics to the K-band spectra:

- The spectra all have similar slopes within the 1.55 - 1.75 μm wavelength range.

- The spectra all contain strongly defined CO absorption bands that are characteristically found in K and M stars (see examples in Lançon & Rocca-Volmerange (1992), Origlia, Moorwood, & Oliva (1993), Dallier, Boisson, & Joly (1996), and Meyer et al. (1998)).

- The spectra contain metal absorption lines, such as the 1.589 μm Si I line and the 1.711 μm Mg I line, that are characteristically found in cooler stars (see Origlia, Moorwood, & Oliva (1993) and Meyer et al. (1998) for examples).

- The spectra contain no Fe II 1.644 μm line emission, which is associated with supernova activity.

We display these 33 “quiescent” K-band spectra in Figure 1 and the corresponding “quiescent” H-band spectra in Figure 2. The uniformity of the spectra is quite striking, especially when they

are compared to samples of other classes of objects. The LIRGs studied in Goldader et al. (1997) or the interacting galaxies studied in Vanzi, Alonso-Herrero, & Rieke (1998), for example, have variable spectral slopes, and the strengths of Brackett- γ and H₂ lines are variable. In contrast, the slopes of the spectra of these quiescent galaxies are uniform, and the relative strengths of absorption features is consistent throughout the group.

3.1. A Composite Quiescent Spectrum

Based on the spectra of these objects, it is very clear that the K-band emission from these objects is dominated entirely by old red stars that dominate the central bulges of these galaxies. We see such a large collection of spectra as an excellent opportunity. By combining these spectra together, we can create a composite “quiescent” spectrum. This quiescent spectrum could then be treated as representing an old red stellar component in the spectra of galaxies where either continuum emission from an AGN source or hot dust or emission lines from young stars or supernovae or are present.

To build a quiescent K-band spectrum, we began by selecting the 32 of the 33 galaxies above that were S0 or spiral galaxies. (NGC 5846 is classified by the Third Reference Catalogue of Bright Galaxies (de Vaucouleurs et al. 1991) (RC3) as an elliptical galaxy and was therefore left out of this analysis. Composite spectra made from only S0s or only spiral galaxies differed a statistically insignificant amount from each other, so we used the S0 and spiral galaxies together.) We first redshift-corrected all of the spectra to the rest frame. Next, we finely resampled the spectra from 2.0 μm to 2.4 μm at intervals of 10^{-4} μm using a spline procedure. We then normalized the spectra and median combined them using the same method we used to normalize and combine the spectra for individual galaxies. A similar procedure was followed to produce quiescent H-band spectra except that the 14 spectra that were used were resampled from 1.55 μm to 1.75 μm at intervals of 10^{-4} μm .

We show the resulting quiescent spectra in Figure 3 and Figure 4. Spectral features, namely the metal absorption lines and the CO bandheads, were identified using spectral line data from Kleinmann & Hall (1986), Wallace & Livingston (1992), and Goorvitch (1994). Tables 4 and 5 list the identified features.

3.2. Analysis with Population Synthesis

To better understand the composite spectrum, we will analyze measurements of features in the spectrum using the Starburst99 (Leitherer et al. 1999) population synthesis models. Starburst99 only considers two star formation scenarios: an instantaneous burst of star formation, and continuous star formation. We will consider both scenarios in our analysis. We used most of the default input choices for Starburst99 with the exception of the initial mass function (IMF). We used solar

metallicities because we assume that the galaxies used to build the composite quiescent spectrum should have similar metallicities to the Milky Way. Although we will primarily focus on model results that depend on using a Salpeter IMF with a slope of 2.35 and an upper mass cutoff of $100 M_{\odot}$, we will also briefly mention the implications of using either an IMF with a slope of 2.35 and an upper mass cutoff of $30 M_{\odot}$ or an IMF with a slope of 3.30 and an upper mass cutoff of $100 M_{\odot}$.

Several different near-infrared spectroscopic indicators are modeled in Starburst99, but only a few of these indicators trace older stellar populations. We will use Starburst99’s predictions of the equivalent widths of the Si 1.59 μm line, the CO 6-3 feature at 1.62 μm , and the CO 2-0 feature at 2.29 μm (Origlia, Moorwood, & Oliva (1993) describe the motivations for using these lines in near-infrared spectral analysis). Table 6 list measurements of these features using the “line” and continuum locations described in Origlia, Moorwood, & Oliva (1993). Errors in the line measurements are dominated not by random errors in the measurements of the spectral lines but in systematic errors related to the wavelength calibration of the spectrum.

3.2.1. The Instantaneous Burst Scenario

Figure 5 shows plots of Starburst99’s predictions of the equivalent widths over time after an instantaneous burst of star formation that produces a Salpeter IMF. The spectral line measurements and errors, overlaid as horizontal lines, all cross the model at two locations in these plots. The most representative times have been determined quantitatively by searching for the location where the χ^2 value is minimized. The χ^2 value for time t is given by

$$\chi(t)^2 = \sum_i \frac{(w_{meas,i} - w(t)_{model,i})^2}{\sigma_{meas,i}^2} \quad (1)$$

where $w_{meas,i}$ is the measured equivalent width for line i , $\sigma_{meas,i}$ is the error in the measurement, and $w(t)_{model,i}$ is the modeled equivalent width at time t .

The first location at ~ 7 Myr seems less likely to be representative of the stellar populations. At this time after the burst, the bluest stars on the main sequence are beginning to evolve into red supergiants, which have atmospheres dominated by molecular and metal absorption lines. However, as massive stars are evolving past the red supergiant phase, supernova activity is quite strong at this point in time, which implies that shock excitation lines such as the Fe II and H₂ emission lines should be quite strong in the composite quiescent spectrum, which is not the case. Furthermore, the stellar populations are evolving rapidly, which would suggest much more variation in the spectral features than what is found among the quiescent galaxies.

The other location at ~ 180 Myr seems to be more representative of the nuclear stellar populations. At this stage in stellar evolution, most massive stars have completely evolved and no longer significantly contribute to the H- or K-band emission in these objects. Neither supernovae

nor ionizing stars are present, so no strong emission lines are expected. What is left is an old, red stellar population that will produce continuum emission that includes metal and molecular absorption features. Origlia & Oliva (2000) do caution that interpretation of stellar populations older than 100 Myr, particularly using near-infrared absorption features, is problematic because of difficulty in modeling asymptotic giant branch stars. We will therefore treat the Starburst99 output as a rough characterization of the actual stellar populations.

Given the approximate age of the system, it is possible to estimate the ratio of K-band luminosity to the mass of the system for this particular case. From Starburst99, a $10^6 M_{\odot}$ system will lose $2.3 \times 10^5 M_{\odot}$ of its mass through stellar winds and supernovae, thus leaving $7.7 \times 10^5 M_{\odot}$ in stars. The K-band absolute magnitude at this time is -13.7 , which corresponds to a power of 6.1×10^{31} W. This gives a K-band luminosity-to-mass conversion factor of $1.3 \times 10^{-26} M_{\odot} \text{ W}^{-1}$.

The other IMFs considered here, which are weighted more strongly towards low mass stars, do produce results that differ from the Salpeter IMF. The age of the stellar population does not change when a smaller upper mass cutoff is used and changes an insignificant amount if an IMF with a steeper slope is used. In these scenarios, however, less of the total initial mass is lost through supernovae or stellar winds because less mass is in stars that would have high mass loss through stellar winds or that would undergo supernovae explosions. This results in the luminosity-to-mass conversion factor varying somewhat among the three IMF scenarios, but it does not vary by orders of magnitude.

In summary, the results from the Starburst99 simulations demonstrate that an old stellar population formed in an instantaneous burst can reproduce the observed composite quiescent spectrum as well as the spectra of the galaxies used to build the quiescent spectrum. Changing the output IMF in Starburst99 will still lead to a stellar population that can reproduce the measured absorption line features.

3.2.2. *The Continuous Star Formation Scenario*

Figure 6 shows plots of Starburst99’s predictions of the equivalent widths over time after the onset of continuous star formation that produces a Salpeter IMF. The spectral line measurements and errors, overlaid as horizontal lines, all cross the model at two locations in these plots. The earlier crossing, at a time of ~ 10 Myr, seems an unreasonable alternative for reasons similar for those given above for the earlier time in the instantaneous burst models. This leaves the later time as a given alternative. In this case, the age of the stellar population is ~ 730 Myr. The reason for this greater age than in the instantaneous burst scenario is that the continuous star formation continuously adds red supergiants with absorption features. Therefore, more time is needed for stars with shallower absorption features to dominate the spectrum and match these measurements.

For a few reasons, the continuous star formation scenario is more problematic than the instantaneous burst scenario. First of all, the Si, CO 2-0, and CO 6-3 equivalent widths do not all

correspond to similar times after the onset of star formation. The Si and CO 2-0 equivalent widths correspond to an age of 600 - 800 Myr, whereas the CO 6-3 equivalent width corresponds to an age of 2 Gyr or later. The discrepancy between the two measurements suggests that the continuous star formation scenario provides the wrong mix of K and M stars to reproduce the stellar population. More importantly, however, the continuous star formation scenario predicts a Brackett- γ equivalent width of $\sim 30 \text{ \AA}$ at $\sim 730 \text{ Myr}$. No Brackett- γ feature within a magnitude of being that strong is evident in the composite quiescent spectrum. Furthermore, no shock excitation lines are observed, even though supernova activity is continuous in this scenario.

Using other IMFs does not solve the problem. Using a steeper IMF or decreasing the upper mass cutoff does improve the match between the measured and modeled absorption features, but the discrepancy among the best corresponding times for each equivalent width measurement persists. Moreover, the other IMF model results still suggest detectable Brackett- γ equivalent widths. We conclude that changing the IMF slightly improves the match between the Starburst99 output and the measurements, but the resulting simulated stellar population still cannot plausibly represent the observed spectra.

3.2.3. *Conclusions from the Analysis with Population Synthesis*

Ultimately, the data suggests that the instantaneous burst scenario can reproduce the spectra we have observed but the continuous star formation scenario cannot. This seems to be consistent with previous studies of nuclear star formation as well (Kennicutt 1998). We will therefore treat the stellar populations of the nuclei of these quiescent galaxies as though they formed in an instantaneous burst 180 Myr ago.

However, these results should be used cautiously. The results should not be interpreted as indicating that all of the stars in the quiescent galaxies' nuclei formed in one burst of star formation 180 Myr ago. Galaxies are known to be older than 180 Myr, and the star formation histories are expected to be more complex. The age should also not be interpreted as an average age, since the line widths do not vary linearly with time. Instead, the age should be treated as a representative value that can be used with the Starburst99 models to approximate the stellar populations that predominate the near-infrared emission. Future refinements in modeling near-infrared absorption features with population synthesis models, the inclusion of more absorption features in the models, and advances in modeling stellar populations beyond 100 Myr will improve the characterization of the ages of the stellar populations in these quiescent systems. For now, however, we will work with these results from Starburst99.

The viability of the instantaneous burst scenario for the quiescent galaxies suggests that sources with H- and K-band emission lines are comprised of a younger starburst embedded within an older stellar population that is similar to the quiescent stellar population. We apply this interpretation throughout the following section.

4. Non-Quiescent Nuclear Spectra

Only the nuclear H- and K-band spectra of eight galaxies exhibited any emission lines. Some of these galaxies are systems with complex stellar structures in their nuclei that we will discuss in detail in the Section 4.2. The other systems have strong line emission from pointlike nuclei; their spectra are presented as they are discussed.

Interestingly, not all nuclei and other structures that produce emission lines have characteristically similar spectra. We discuss a few of the qualitative variations below, and we provide Table 7 to show how the spectra differ quantitatively. In most cases, the underlying continua and absorption lines for these systems closely matches the quiescent composite spectra derived above with some minor exceptions in the slope of the spectra. This implies that any recent starburst activity lies deeply buried within an older population of evolved stars.

4.1. Types of Non-Quiescent Spectra

In NGC 289, NGC 5713, and part of the nuclear regions of NGC 4100, strong H_2 lines, Brackett- γ lines, and Fe II lines (when H-band data are available) were detected. Otherwise, the galaxies' H- and K-band spectra almost match the quiescent composite spectra. Figures 7 and 8 show the spectra for NGC 289 and NGC 5713 with the quiescent H- and K-band spectra overlaid. (Spectra and data for NGC 4100 are presented in Section 4.2.) At this stage in galaxy evolution, it appears that these systems are seen at a time during which ionizing stars have not completely evolved off the main sequence but supernovae are occurring. According to simulation results from Starburst99, these conditions are met for an instantaneous burst in the 3.5 - 8 Myr age range for a Salpeter IMF.

The A cluster in NGC 1569, part of the nuclear region of NGC 3556, and the nucleus of NGC 4088 exhibit strong Brackett- γ lines but nondetectable H_2 and Fe II lines (when H-band data are available). He I lines may also be present, although it may be relatively weak compared to the hydrogen emission. This helium emission may be a qualitative tracer of O type stars with very strong winds (Kudritzki 1998). The spectrum of NGC 4088 is plotted in Figure 9. (NGC 1569 and NCG 3556 are discussed in more detail in Section 4.2.) The recombination lines indicate that young ionizing stars are present, but the lack of shock excitation lines suggests that the stellar population has not evolved to a point where supernovae are generating shocks in the interstellar medium. Therefore, using Starburst99 data, the stellar population must be less than 3.5 Myr old.

Finally, the galaxies NGC 5005 and NGC 5033 exhibit strong H_2 and Fe II lines from shock excitation but either weak or nonexistent Brackett- γ emission. Interestingly, the K-band continua of these galaxies do not match the composite quiescent spectrum. The slopes of the two galaxies differ from the quiescent spectrum, and the observed CO bands in NGC 5033 are shallower than most other galaxies. However, the continua can be fit by a linear combination of the composite

quiescent spectrum and a power law. Table 8 provides basic data on the underlying power laws in the K-band. Note that these power law fits are only approximations as they are highly sensitive to the exact regions of the K-band continuum used in the fits. Figures 10 and 11 show the spectra for these galaxies along with the best fitting continua.

The absence of strong recombination lines indicates that NGC 5005 and NGC 5033 have at least evolved past 8 Myr. If the shock excitation lines are interpreted as originating from supernovae, then we could conclude that the stellar populations in these galaxies are in the 8 - 36 Myr age range. However, these two galaxies are interacting with each other (Helou, Salpeter, & Terzian 1982). The shock excitation lines may simply be tracing cloud collisions from interaction-induced gas infalls into these galaxies' nuclei. Since NGC 5005 is classified as a LINER and NGC 5033 is classified as a Seyfert (Ho, Filippenko, & Sargent 1997b) (HFS97b), another possibility is that the shock excitation lines are the results of gas outflows from AGN. The presence of additional continuum emission could be further proof of AGN in these galaxies. However, when we discuss the near- and mid-infrared colors and luminosities in Section 5, we will discuss additional evidence that the shock excitation lines may arise from supernovae.

4.2. Extranuclear Targets and Complex Nuclear Targets

In this section, we discuss unusual targets with either complex nuclear structure or unusual star clusters outside their nuclei that also had spectra taken. All of the galaxies listed below produce detectable emission lines in at least one location.

4.2.1. NGC 1569

NGC 1569 contains two prominent star clusters. These star clusters are identified in Figure 12. This is a well-studied system where the stellar populations have been identified (Greggio et al. 1998; Maoz, Ho, & Sternberg 2001; Aloisi et al. 2001; Origlia et al. 2001), so these observations provide few new insights into the galaxy itself. However, the results should be considered within the context of the sample as a whole, particularly since this is one of the few galaxies in the sample where emission lines have been detected in the spectroscopy.

Figures 13 and 14 present the spectra of NGC 1569A and NGC 1569B. NGC 1569A exhibits strong Brackett- γ emission and He II emission but no detectable Fe II or H₂ emission. NGC 1569B, however, produces no strong near-infrared emission lines. Otherwise, NGC 1569A, along with NGC 1569B, have similar continua with similar absorption features.

At first glance, the H and K continua appear to match the composite quiescent spectrum very well. However, a closer look at the spectral line emission indicates that the absorption features in the NGC 1569 spectra do not match the composite quiescent spectrum. Note, for example, the missing Al I and Mg I features near 2.11 μm and the apparent absence of the Ca I triplet near 2.26 μm .

These lines may all be missing because NGC 1569, as a dwarf, has a lower metallicity than most nearby spiral galaxies. Furthermore, note the deeper CO features in the spectrum of NGC 1569B. This indicates that the B cluster may contain higher-mass red giants than the average galactic nucleus and that it may be younger than 180 Myr.

Nonetheless, the data imply that a starburst less than 3.5 Myr old is embedded within an older stellar population in NGC 1569A and that NGC 1569B consists of an older stellar population. These results are consistent with most previous studies. The lack of detection of shock excitation lines in the near-infrared spectra is also consistent with Greve et al. (2002), which did not detect any supernovae at radio wavelengths.

4.2.2. *NGC 3556*

The nuclear region of NGC 3556 contains two regions of similar surface brightness but different shape. Figure 15 shows a K-band image of these regions, which we will refer to as the east and west nuclear regions of NGC 3556. Although the two regions are relatively close to each other, their K-band spectra are stunningly different.

Figure 16 shows the spectra of the east and west nuclear regions, with the composite quiescent spectrum overlaid on each spectrum. The underlying continua for both objects has the same slope as the composite quiescent spectrum and do feature similar CO absorption features, although most other absorption features are so poorly distinguished that the match between the spectra and the composite is not as clear as in other cases. The east nuclear region appears to be a relatively quiescent region. The west nuclear region, however, exhibits strong He I and Brackett- γ line emission that implies the presence of a stellar population that is less than 3 Myr old.

4.2.3. *NGC 4100*

Based on images and information from the literature, NGC 4100 seems to be an unspectacular Sbc galaxy with neither Seyfert nor LINER nuclear activity (HFS97b). A close examination of the nucleus in the K-band, however, reveals that the nucleus actually has a knotted structure, as seen in Figure 17. The spectroscopy of the target also produces some intriguing results, as seen in Figure 18. The K-band spectrum of the center of the galaxy simply appears quiescent. The spectrum of the region just south of the center of the galaxy, however, reveals the presence of detectable Brackett- γ and molecular hydrogen emission. Gas falling into the nucleus of this galaxy may have created the star formation structure in this galaxy’s center. Given the complexity of the structure, we suggest that the nucleus of NGC 4100 should be observed with an integral field spectrometer so as to better understand the locations of photionizing stars, evolved red stars, and shocks in the system as well as to determine the overall masses in young and old stars.

The complex nuclear star formation region of NGC 4100 may be significantly more extended than the slit used for the observations. Therefore, we have declined to use NGC 4100 in any of the quantitative analysis, and we do not report any emission line equivalent widths or luminosities. However, we still use NGC 4100 qualitatively in the discussion.

4.2.4. NGC 5676

The observations of NGC 5676 not only allowed us to examine the spectra of the nucleus but also of a bright knot of star formation north of the nucleus. This knot stood out prominently in the $12\ \mu\text{m}$ image presented in Paper 1. At that wavelength, the surface brightness of the northern knot was higher than the surface brightness of the nucleus. This strongly contrasts with the K-band image of the galaxy, where the nucleus clearly has a surface brightness that is higher than any region within the disk even though the northern knot is a prominent source of K-band emission in the disk. Clearly, some kind of extraordinary star formation event is taking place in the northern knot. The K-band spectroscopy reveals more clues as to exactly what is happening.

Figure 19 shows the K-band spectrum of the the northern knot of NGC 5676. The region produces very strong Brackett- γ and He I emission that dominates the K-band emission. Otherwise, no other emission or absorption features are discernable in the northern knot’s spectrum. The presence of the He I lines and the lack of H₂ shock excitation lines suggests that this system is younger than 3 Myr.

Clearly, the northern knot is a large, young star formation complex that may represent an important stage in the evolution of disk stars not only in NGC 5676 but in other galaxies as well. Further spectroscopic observations of the complex would allow for the calculation of the total mass of this system and could even be used to look for dynamical clues as to how this complex formed.

4.3. Morphological, Environmental, and AGN Characteristics

The occurrence of H- and K-band emission lines in only a few galaxies leads us to examine what factors lead to the production of these features. We will consider morphological and environmental factors that could possibly be triggers or conditions for the star formation activity we observed. We will also discuss the implications of our results for better understanding AGN activity, particularly LINERs.

4.3.1. Morphological Characteristics

From looking at the morphological types of all the non-quiescent galaxies, it is clear that location along the Hubble sequence is a major factor. Of the eight non-quiescent galaxies, all of them are classified in RC3 as Sbc galaxies or later types. This clearly supports the paradigm that the relative strength of star formation increases along the Hubble sequence, even though Kennicutt (1998) states that this trend is primarily one seen in the disks of spiral galaxies, not in their nuclei. The finding agrees with the photometric results reported in Paper 2. This also agrees well with the results presented in (Mannucci et al. 2001), where composite near-infrared spectra made for different morphological types of galaxies show that recombination and shock excitation line emission is most prominent in late-type galaxies.

The results presented here probably reflect the change along the Hubble sequence in the relative contributions of bulge stars to the H- and K-band emission. In S0s and early-type spiral galaxies, which are defined as having large bulges, the bulge stars dominate the near-infrared emission. If any star formation was present, the recombination line emission is relatively insignificant compared to the bulge star continuum emission and therefore extremely difficult to detect. In late-type spiral galaxies, however, fewer bulge stars are present by definition. Therefore, if star formation is present, the lower continuum from the bulge stars

allows for the detection of recombination lines.

Nonetheless, not all late-type spiral nuclei produce detectable Brackett- γ or shock excitation line emission, as quite a large number of the near-infrared spectra of Sbc - Scd galaxies are quiescent. Although location along the Hubble sequence is a necessary factor for the H- and K-band line emission, it appears to not be a sufficient factor.

Bars have often been suggested as a means by which gas may be funneled into the nuclei of galaxies, thus leading to enhanced star formation (Noguchi 1988; Athanassoula 1992; Wada & Habe 1992; Friedli & Benz 1993; Heller & Shlosman 1994; Wada & Habe 1995). Several studies have found a difference between the nuclear star formation activity of barred and unbarred spiral galaxies, although the differences are mainly seen in early type galaxies (Devereux 1987; Huang et al. 1996; Ho, Filippenko, & Sargent 1997a; Roussel et al. 2001). Six of the eight non-quiescent galaxies in this sample are at least weakly barred according to RC3, although only three are identified as strongly barred. However, two of the galaxies are identified as unbarred: NGC 4100 and NGC 5033. The K-band image of NGC 4100 in Paper 1 hints at the possibility of a bar, but NGC 5033 is unquestionably unbarred. Given that many of these non-quiescent galaxies are only weakly barred and that at least one is unbarred, it seems as though bars are not absolutely necessary for triggering nuclear star formation. Furthermore, some of the observed late-type barred spiral galaxies have quiescent near-infrared spectra, suggesting that bars do not directly correspond to enhanced star formation activity.

4.3.2. *Interaction History*

Interactions have been proposed as a means of triggering or enhancing star formation in the nuclei of galaxies by driving gas inward, even before the interacting galaxies begin to merge (Mihos & Hernquist 1996). Observations of nuclear star formation confirm these effects (Keel et al. 1985; Cutri & McAlary 1985; Kennicutt et al. 1987; Wright et al. 1988).

In the non-quiescent galaxies in this sample, four of them are interacting. NGC 289 is interacting with a dwarf companion (Arp 1981), NGC 4088 is interacting with NGC 4085 (van Moorsel 1983), and NGC 5005 and NGC 5033 are interacting with each other (Helou, Salpeter, & Terzian 1982). The nuclear star formation activity in the three interacting barred galaxies could just as easily be explained as being caused by the interaction as it is explained as being caused by the bar, especially in light of such studies as Noguchi (1988) that discuss bars forming in interactions and causing gas infall. For NGC 5033, which is unbarred, the interaction is the only obvious mechanism for explaining why signs of star formation (or at least shocked gas) are found in the nucleus.

What is particularly interesting is that NGC 5005 and NGC 5033 have very similar spectra. If the shock excitation line emission from these two galaxies is interpreted as coming from supernovae produced from starburst events, then the events may have occurred nearly-simultaneously in both galaxies. This would be a powerful demonstration of the effects of interactions on nuclear star formation activity if it could be confirmed.

Two additional non-quiescent galaxies, NGC 1569 and NGC 5713, have lopsided, amorphous appearances. that suggest that they may have experienced recent minor merger events. Such minor merger events are capable of enhancing nuclear star formation activity (Mihos & Hernquist 1994; Hernquist & Mihos 1995; Rodnick, Rix, & Kennicutt 2000). Therefore, we would suggest that these galaxies have recently undergone

minor mergers that has triggered their nuclear star formation activity.

These results demonstrate that interactions are as important as bars in triggering nuclear star formation activity. NGC 3556 and NGC 4100, however, are examples of non-interacting systems with current nuclear star formation, which demonstrates that interactions are sufficient but not necessary for triggering nuclear bursts. Moreover, not all interacting galaxies show near-infrared spectroscopic signs of recent star formation activity. Several of the quiescent galaxies in this sample are also interacting, including NGC 1512 (Hawarden et al. 1979), NGC 4725 (Haynes 1979), NGC 5457 (Davies, Davidson, & Johnson 1980), NGC 5566 (Helou, Salpeter, & Terzian 1982), NGC 5746 (Sandage, & Bedke 1994), NGC 5846 (Sandage, & Bedke 1994), NGC 5866 (Sandage, & Bedke 1994), and NGC 5907 (Sandage, & Bedke 1994). Many, but not all, of these quiescent interacting galaxies are early type spirals with large bulges. Mihos & Hernquist (1994) demonstrated that large bulges can inhibit the infall of nuclear gas into galactic nuclei during interactions, which may explain why most of the interacting quiescent galaxies in this sample do not exhibit nuclear near-infrared line emission.

4.3.3. *AGN Characteristics*

The relation between the AGN activity (as determined from optical spectroscopy) and the H- and K-band spectroscopy can provide additional clues in understanding the underlying mechanisms behind the nuclear activity.

In Seyferts, the question has been how the AGN activity may be related to star formation. Several studies, including ultraviolet and optical observations (Gonzalez-Delgado & Perez 1993; Heckman et al. 1997; González Delgado et al. 1998; González Delgado, Heckman, & Leitherer 2001), near-infrared spectroscopic surveys (Oliva et al. 1995, 1999), far-infrared surveys (Rodriguez Espinosa, Rudy, & Jones 1987; Dultzin-Hacyan, Moles, & Masegosa 1988), and CO surveys (Heckman et al. 1989) have found evidence for relatively recent circumnuclear star formation in Seyfert 2 galaxies. Seyfert 1 galaxies show no signs of being associated with star formation activity, although intermediate classes between 1 and 2 may be. The emerging paradigm suggests that Seyfert 2 activity appears on the order of 10 Myr after an instantaneous starburst. According to Starburst99, supernova activity should be prevalent, near-infrared recombination lines will be undetectable, and absorption features will generally be deeper than average. However, some infrared surveys of Seyferts, such as Oliva et al. (1995), Oliva et al. (1999), and Hill et al. (1999) note that the absorption features could be diluted by continuum emission from the AGN. Nonetheless, these studies have presented us with a model that can be compared to observations.

In LINERs, near-infrared spectroscopy is particularly important. With both photoionization and shock excitation lines, more constraints can be placed on whether the optical spectra of LINERs are produced by photoionization by either clusters of young stars (Terlevich & Melnick 1985; Shields 1992) or AGN (Ho, Filippenko, & Sargent 1993) or by shock excitation from supernovae produced in a starburst or AGN (Heckman 1980). As has been discussed by Alonso-Herrero et al. (1997), near-infrared Fe II and recombination lines can be the key to distinguishing between shock excitation and photoionization results.

We will rely on the classifications of HFS97b in this discussion. Two of the eight non-quiescent galaxies in this sample are not classified by HFS97b, although the NASA/IPAC Extragalactic Database lists one of them as an H II galaxy. Four of the six non-quiescent galaxies are also identified by HFS97b as H II galaxies. This leaves one Seyfert (NGC 5033) and one LINER (NGC 5005) as AGN with detected H and K spectral

line emission.

Only two galaxies observed in this spectroscopic survey were classified as Seyferts by HFS97b. The near-infrared spectrum of NGC 4725 was quiescent. HFS97b, however, state that the classification of NGC 4725 is uncertain; perhaps the non-detection of emission lines along with the lack of a continuum that dilutes the absorption features indicates that this galaxy is not a Seyfert. The near-infrared spectrum of NGC 5033, however, exhibited weak but broad Brackett- γ emission as well as strong shock excitation line emission. The broad Brackett- γ line clearly indicates the presence of an AGN. The shock excitation lines, however, could be interpreted as originating from the AGN, from the interaction with NGC 5005, or from a circumnuclear starburst. If it is a circumnuclear starburst, this would show the same kind of association between Seyfert optical spectral activity and star formation activity that had been found previously. Unfortunately, this sample lacks enough Seyferts to really make a definitive statement about them, although many other surveys in the literature (see references in Section 1) could make stronger statements.

Seven of the galaxies in this spectroscopic sample were classified as LINERs by HFS97b. Another nine were classified as transition objects, which may be more closely related to LINERs than to other classes of objects. However, near-infrared emission lines were only detected in one of these 16 objects, NGC 5005. This is a relatively low rate of detection compared to the H II galaxies, where 4 of 13 galaxies in the sample classified as such by HFS97b had detected near-infrared line emission. However, these results are consistent with other studies; Larkin et al. (1998) and Sosa-Brito, Tacconi-Garman, & Lehnert (2001) also present near-infrared LINER spectra that have no detectable emission lines.

In NGC 5005, the characteristic strong shock excitation lines, particularly the Fe II lines, and the absence of recombination lines are consistent with other near-infrared spectroscopy observations of LINERs (Larkin et al. 1998; Alonso-Herrero et al. 2000). In this target, it is obvious that shocks are propagating through the nucleus, photoionization is relatively weak, and therefore the optical LINER emission is probably generated by shock excitation.

In the other 13 objects, though, the absence of all near-infrared emission lines and the close match between the near-infrared spectra of these galaxies and the near-infrared spectra of other quiescent galaxies indicate that the spectra are dominated by evolved red stars. If shock excitation or photoionization by hot young stars is taking place in the nuclei of these LINERs, the emission is weak compared to the continuum emission from the older quiescent stellar populations. If the non-detection of near-infrared spectral lines are interpreted as the absence of shocks or star formation, then only weak AGN may be responsible for the optical emission line spectra.

The relatively low nuclear 12 μ m flux to K-band flux ratios determined for the galaxies in this sample in Paper 2 also indicated that nuclear star formation is relatively weak in LINERs and transition objects compared to H II galaxies. These additional spectroscopic observations demonstrate that evolved red stars dominate the near-infrared emission in these systems and that photoionization from star formation is unlikely to be causing the optical LINER emission observed in these galaxies.

4.4. Ratio of Young to Old Stellar Mass

4.4.1. Determination of the Young Stellar Mass

The total mass formed within the most recent starburst event can be determined using measurements of the Brackett- γ or Fe II 1.644 μm luminosities. We will use data from Starburst99 to determine the conversion factors from these line luminosities to young stellar masses. We treat the star formation as though it takes place in an instantaneous burst. We assume that the metallicities are solar and that the IMF of the burst has a slope of 2.35 and an upper mass cutoff of 100 M_{\odot} . Note that, for convenience, the data used to calculate the conversion values correspond to a simulated burst that forms $10^6 M_{\odot}$ in stars. The luminosities and masses presented below are dependent on the initial mass, but the final conversion factors are mass-independent.

We will begin by finding conversion factors between Brackett- γ luminosity and total young stellar mass. As we stated above in discussing the ages of the young stellar populations, the appearance or nondetection of certain spectral lines indicate different ages for the systems. We therefore divide the galaxies with Brackett- γ line detections into two categories: pre-supernova systems (systems with ages of 0.0 - 3.5 Myr that exhibit no shock excitation lines) and supernova systems with recombination line emission (systems with ages of 3.5 - 8.0 Myr that have detectable shock excitation lines). Table 9 presents Starburst99 data on the range and median value of Brackett- γ luminosities, the stellar masses remaining in the systems, and the conversion factors from Brackett- γ luminosities to masses for these two types of systems. Note that the large change in the Brackett- γ luminosities in the 3.5 - 8.0 Myr range mean that the young stellar masses determined from the line luminosities will only be accurate to within a factor of 10.

To use the Fe II 1.644 μm emission lines to trace young stellar masses, we must select a conversion factor that changes supernova rates into Fe II line luminosities. We will use 1.2×10^{34} W yr, which was determined by Alonso-Herrero et al. (2003). This agrees within a factor of 2 with the conversion factor of 1.9×10^{34} W yr determined in van der Werf et al. (1993) (using their assumptions on the scalar factor ν and assuming that their $(E_0/10^{51}$ erg) term is equal to unity). These conversion factors, however, disagree with the conversion factor of 1.7×10^{33} W yr determined in Colina (1993) (using their assumptions presented about the Fe II luminosity of supernova remnants and the duration of Fe II emission). However, Alonso-Herrero et al. (2003) and references therein state that the Fe II emission should last longer than what is assumed in Colina (1993), which could partly explain why the Colina (1993) conversion factors are inconsistent with other values.

As with the galaxies with Brackett- γ emission, galaxies with Fe II emission can be split into two groups: supernova systems with recombination line emission (which have ages of 3.5 - 8.0 Myr) and supernova systems without recombination line emission (which have ages of 8.0 - 36 Myr). Table 10 presents data on the range and median of supernova rates, the corresponding median Fe II 1.644 μm line luminosities, the total stellar mass remaining in the systems, and the line luminosity-to-mass conversion factors.

To calculate the ratios of young to old stars in the non-quiescent galaxies using the K-band flux to trace the older stars, we will need to subtract the total contribution of the young stars. The K-band flux within younger stars can simply be determined by multiplying the Brackett- γ and Fe II line fluxes by ratios of the K-band continuum fluxes to line fluxes predicted by Starburst99. Table 11 presents these data for the three different age ranges discussed above. Note that these correction factors are only good to within a factor of 10, mainly because the K continuum flux varies by a factor of 10 within the selected time periods. However, as we will see below, these values will work for the science that we are doing.

4.4.2. *Determination of the Young to Old Stellar Mass Ratios*

Using the K continuum luminosity to old stellar mass conversion factor derived in Section 3.2 and these conversion factors between line luminosities and young stellar mass, we can now measure both the mass produced in these nuclear star formation events (for at least the regions falling within the slit) and the ratio of young stellar mass to total stellar mass in the nuclei of these galaxies. For objects such as Cluster A in NGC 1569, the west nuclear region in NGC 3556, and the northern knot in NGC 5676, we will treat the underlying continuum as though it originates from an evolved stellar population of solar metallicity for simplicity, even though this may not be entirely accurate.

Table 12 lists the masses of young and old stars within the non-quiescent systems and the ratio of the masses as well as all of the parameters needed to calculate the masses. Note that the luminosities and masses in Table 12 are for the region that falls within the spectrometers’ slits and may not necessarily reflect the true total luminosities and masses for the nuclear star forming regions if the regions are extended. The results demonstrate that a strong star formation event could produce up to 5 % of the stellar mass found within a galaxy’s nucleus. The data also demonstrate that we were able to detect star formation within galaxies where the young stars accounted for less than 0.03 % of the total mass, but typically young stars make up ~ 2 % of the nuclear stellar mass in a non-quiescent galaxy. The young stars also contribute appreciably to the K-band luminosities of these galaxies’ nuclei. In some cases, the young stars contribute more than 10 % of the flux in the K-band.

These ratios of young to old stellar mass agree with an overall picture of nuclear stellar populations being formed in a series of instantaneous bursts. Consider that 20 % of the galaxies in this sample have recently increased their central masses by 2 %. These young stellar masses formed within the past 36 Myr. This means that the mass of the average galaxy’s nuclear population increases by ~ 0.4 % over a period of 36 Myr. The age of the universe is ~ 14 Gyr. Therefore, if the nuclear stellar masses are being increased continuously over time, then 36 Myr / 14 Gyr of the mass, or 0.25 %, of the stellar mass should have been created within the past 36 Myr in the average galaxy. Despite the number of approximations in this calculation, these two percentages are consistent with each other, which supports the paradigm of nuclear star formation occurring as instantaneous bursts spread over the lifetime of the galaxy.

The data also place the northern knot of NGC 5676 into an interesting context. The mass of stars being formed within the northern knot and the percentage of mass in new stars is comparable to those values for nuclear bursts of star formation. Although nuclear star formation is very important in nearby galaxies, this star formation event in NGC 5676 highlights the importance of not ignoring the role of extranuclear bursts of star formation in galactic evolution.

As a more technical achievement, the analysis for both the Brackett- γ and Fe II lines produce similar results in the two galaxies in this analysis. For NGC 289, the two young stellar masses calculated from the two lines are within a factor of 3 of each other. For NGC 5713, however, the results agree to within 20 %. This demonstrates that our methods for calculating young stellar masses are at least internally consistent. However, it is quite a spectacular achievement, especially given some of the order of magnitude uncertainties in the interpretation of the Starburst99 data.

5. Comparison of Quiescent and Non-Quiescent Galaxies in Mid-Infrared / K Color-Luminosity Plots

In Paper 2, we justified using mid- and far-infrared fluxes divided by near-infrared fluxes as a tracer of star formation activity by examining the ratios that were predicted by Starburst99. As a test of these tracers, we will compare the colors and luminosities of the quiescent and non-quiescent galaxies to each other.

Figure 20 shows a plot of the $\frac{f_{MIR}}{f_K}$ colors for the inner 15'' of the galaxies in the spectroscopic subsample against both the mid-infrared and the K-band luminosities from the same regions. Galaxies with quiescent and non-quiescent nuclear spectra are represented as different symbols on the plots. The detection of spectral line emission is not correlated with luminosity in either waveband. However, when the non-quiescent systems with only shock emission lines are excluded, it appears that ratios like the $\frac{f_{MIR}}{f_K}$ ratio are well correlated with the detection of recombination lines in the near-infrared, although the correlation is not perfect. When the K-S test is applied in comparing the quiescent versus non-quiescent $\frac{f_{MIR}}{f_K}$ ratios, the resulting fractional probability that the two data sets came from the same samples is 0.026. However, when the galaxies producing only shock excitation line emission are left out of the non-quiescent sample, the K-S test determines the probability as 0.0032. This is a strong statistical demonstration that shows the relation between systems producing strong Brackett- γ emission and systems with high $\frac{f_{MIR}}{f_K}$ ratios.

Three of the non-quiescent galaxies, however, occupy locations in these color-magnitude diagrams where their colors are close to the mean value but where their luminosities are relatively high compared to galaxies with similar colors. All three of these galaxies have strong shock excitation line emission, which could imply that supernovae are present. Now, consider Figure 2 in Paper 2. For an instantaneous burst, any tracer of the bolometric luminosity (such as the 12 μm emission, which is discussed in Paper 2) when normalized by the K-band emission will drop sharply when massive main sequence objects evolve into red supergiants. The low colors are found at ~ 8 Myr, when supernova activity is also strong. Therefore, supernovae could be responsible for producing the observed shock emission lines in these systems as well as reduced $\frac{f_{MIR}}{f_K}$ ratios and the relatively high luminosities observed in these galaxies.

In summary, the $\frac{f_{MIR}}{f_K}$ ratio appears to be well correlated with strong photoionization emission in the near-infrared, although it is not correlated with strong shock excitation emission. Therefore, mid-infrared fluxes, as well as the correlated far-infrared fluxes, can be used to trace star formation activity when normalized by K-band fluxes.

6. Conclusions

6.1. Summary of Results

In this sample, 33 of the 41 galaxies nuclei were found to have quiescent spectra. These spectra consisted of continuum emission with many metal and CO absorption lines, which are characteristic of evolved red stars. Using Starburst99, we found that the composite spectrum made from these quiescent galaxies' spectra was best represented by an instantaneous burst that took place ~ 180 Myr ago, although we caution that this is not necessarily supposed to reflect the true star formation history. We found few differences between using Salpeter and other IMFs, but we did find that the continuous star formation scenario failed to reproduce the observed equivalent widths.

The remaining 8 galaxies have nuclear spectra that include emission lines. In many cases, the underlying continuum exhibited the same slope and contained the same absorption features that were present in the composite quiescent spectra. On top of this quiescent continuum, the galaxy may produce either photoionization lines such as Brackett- γ and He I emission, shock excitation lines such as H₂ lines and Fe II emission, or both. The lines present would reflect the age of the young stellar population, with photoionization lines present up to 8 Myr after a burst and shock excitation lines present from 3.5 to 36 Myr after a burst. Some of the systems showed relatively point-like spectral line emission, whereas others exhibited emission in complex structures. One galaxy, where the nuclear emission was quiescent, had a strong extranuclear starburst that was detected and included in some parts of the analysis.

These non-quiescent galaxies share many characteristics. All of them are Sbc galaxies or later, which suggests that these instantaneous nuclear bursts are more likely in the later-type galaxies. 6 of the 8 galaxies were definitely barred, which suggested that bars may play a role in triggering nuclear star formation. However, 6 of the 8 galaxies either were interacting or had been involved in interactions, which suggests that interactions are just as important as bars in triggering nuclear star formation. In relation to AGN activity, it appears that most non-quiescent galaxies are H II galaxies and that most LINERs and transition objects are quiescent.

The average ratio of young to old stellar masses for the non-quiescent systems was found to be $\sim 2\%$. Given that these 2% enhancements occur in $\sim 20\%$ of the galaxies in the sample, these enhancements are found to be consistent with nuclear stellar populations forming through a series of instantaneous bursts.

Finally, we found that the $\frac{f_{MLR}}{f_K}$ ratios functioned very well in separating non-quiescent galaxies from quiescent galaxies. The exception was with galaxies that contained only shock excitation lines, but the ratio was expected to decrease significantly for these galaxies.

The data and results presented here now form a baseline for comparison to other galaxies with more exotic star formation or AGN activity. Furthermore, the composite quiescent spectra and the conversion factors developed here should provide additional analysis tools for studying enhanced star formation activity.

6.2. Future Work

While the spectroscopy presented here surveys a range of different kinds of galaxies, it is only a limited sample. A broad range of morphologies were included in the sample, but not a broad range of AGN types; the spectroscopic sample only contained two Seyferts. Furthermore, as Virgo Cluster galaxies were left out of the original sample, no data are available for comparing field and cluster galaxies. A larger near-infrared spectroscopic survey of a complete, volume-limited sample of galaxies would provide additional constraints on these stochastic bursts of star formation, such as the frequency of their occurrence, their relation to bars, environment, Seyfert activity, and LINER activity, and the range of masses formed within these bursts.

Single slit spectrometers are good for sampling the pointlike nuclei of many nearby galaxies and can return spectroscopic data that accurately represent the stellar populations and total star formation activity within these galaxies. However, when the nuclear star formation structures become more complex, as is the case for NGC 3556 and NGC 4100, then a single slit could possibly miss much of the spectral line emission coming from within the centers of these galaxies. Therefore, integral field near-infrared spectroscopic surveys of nearby spiral galaxies would appear to be warranted. Such a survey would not only provide more accurate data on the stellar populations and total line emission from the nuclei of galaxies but also provide data on

the number of galaxies with complex, extended nuclear structures that could lead to additional clues on the phenomenology of nuclear star formation activity.

GJB would like to thank Barry Rothberg, John Rayner, and Mark Seigar for their assistance during observing; Michael Cushing for his help on data processing; Almudena Alonso-Herrero, Charles Engelbracht, Elizabeth Barton Gillespie, Robert C. Kennicutt, and Michael Meyer for their helpful discussions on the analysis. This research has been supported by NASA grants NAG 5-3370 and JPL 961566.

REFERENCES

- Alonso-Herrero, A., Rieke, M. J., Rieke, G. H., & Ruiz, M. 1997, *ApJ*, 482, 747
- Alonso-Herrero, A., Rieke, M. J., Rieke, G. H., & Shields, J. C. 2000, *ApJ*, 530, 688
- Alonso-Herrero, A., Rieke, G. H., Rieke, M. J., & Kelly, D. M. 2003, *AJ*, 125, 1210
- Aloisi, A., et al. 2001, *AJ*, 121, 1425
- Arp, H. 1981, *ApJS*, 46, 75
- Athanassoula, E. 1992, *MNRAS*, 259, 345
- Bendo, G. J., et al. 2002a, *AJ*, 123, 3067 (Paper 1)
- Bendo, G. J., et al. 2002b, *AJ*, 124, 1380 (Paper 2)
- Boisson, C., Coupè, S., Cuby, J. G., Joly, M., & Ward, M. J. 2002, *A&A*, 396, 489
- Burston, A. J., Ward, M. J., & Davies, R. I. 2001, *MNRAS*, 326, 403
- Colina, L. 1993, *ApJ*, 411, 565
- Coziol, R., Doyon, R., & Demers, S. 2001, *MNRAS*, 325, 1081
- Cutri, R. M., & McAlary, C. W. 1985, *ApJ*, 296, 90
- Dallier, R., Boisson, C., & Joly, M. 1996, *A&AS*, 116, 239
- Davies, R. D., Davidson, G. P., & Johnson, S. C. 1980, *MNRAS*, 191, 253
- de Vaucouleurs, G., de Vaucouleurs, A., Corwin, H. G., Buta, R. J., Paturel, G., & Fouque, P. 1991, *Third Reference Catalogue of Bright Galaxies* (Berlin: Springer-Verlag) (RC3)
- Devereux, N. 1987, *ApJ*, 323, 91
- Dultzin-Hacyan, D., Moles, M., & Masegosa, J. 1988, *A&A*, 206, 95
- Engelbracht, C. W. 1997, Ph.D. thesis, University of Arizona
- Forbes, D. A., & Ward, M. J. 1993, *ApJ*, 416, 150
- Förster Schreiber, N. M. 2000, *AJ*, 120, 2089
- Friedli, D., & Benz, W. 1993, *A&A*, 268, 65
- Goldader, J. D., Joseph, R. D., Doyon, R., & Sanders, D. B. 1995, *ApJ*, 444, 97
- Goldader, J. D., Joseph, R. D., Doyon, R., & Sanders, D. B. 1997, *ApJS*, 108, 449
- Gonzalez-Delgado, R. M., & Perez, E. 1993, *Ap&SS*, 205, 127
- González Delgado, R. M., Heckman, T., Leitherer, C., Meurer, G., Krolik, J., Wilson, A. S., Kinney, A., & Koratkar, A. 1998, *ApJ*, 505, 174
- González Delgado, R. M., Heckman, T., & Leitherer, C. 2001, *ApJ*, 546, 845
- Goorvitch, D. 1994, *ApJS*, 95, 535
- Greenhouse, M. A., Woodward, C. E., Thronson, H. A., Rudy, R. J., Rossano, G. S., Erwin, P., & Puetter, R. C. 1991, *ApJ*, 383, 164

- Greenhouse, M. A., et al. 1997, *ApJ*, 476, 105
- Greggio, L., Tosi, M., Clampin, M., De Marchi, G., Leitherer, C., Nota, A., & Sirianni, M. 1998, *ApJ*, 504, 725
- Greve, A., Tarchi, A., Hüttemeister, S., de Grijs, R., van der Hulst, J. M., Garrington, S. T., Neininger, N. 2002, *A&A*, 381, 825
- Hawarden, T. G., van Woerden, H., Mebold, U., Goss, W. M., & Peterson, B. A. 1979, *A&A*, 76, 230
- Haynes, M. P. 1979, *AJ*, 84, 1830
- Heckman, T. M. 1980, *A&A*, 87, 152
- Heckman, T. M., Blitz, L., Wilson, A. S., Armus, L., & Miley, G. K. 1989, *ApJ*, 342, 735
- Heckman, T. M., Gonzalez-Delgado, R., Leitherer, C. Meurer, G. R., Krolik, J., Wilson, A. S., Koratkar, A., & Kinney, A. 1997, *ApJ*, 482, 114
- Heller, C. H., & Shlosman, I. 1994, *ApJ*, 424, 84
- Helou, G. H., Salpeter, E. E., & Terzian, Y. 1982, *AJ*, 87, 1443
- Hernquist, L., & Mihos, C. J. 1995, *ApJ*, 448, 41
- Hill, T. L., Heisler, C. A., Sutherland, R., & Hunstead, R. W. 1999, *AJ*, 117, 111
- Ho, L. C., Filippenko, A. V., & Sargent, W. L. W. 1993, *ApJ*, 417, 63
- Ho, L. C., Filippenko, A. V., & Sargent, W. L. W. 1997a, *ApJ*, 487, 591
- Ho, L. C., Filippenko, A. V., & Sargent, W. L. W. 1997b, *ApJS*, 112, 315 (HFS97b)
- Huang, J. H., Gu, Q. S., Su, H. J., Hawarden, T. G., Liao, X. H., & Wu, G. X. 1996, *A&A*, 313, 13
- Ivanov, V. D. 2000, Ph.D. thesis, University of Arizona
- Keel, W. C., Kennicutt, R. C., Hummel, E., & van der Hulst, J. M. 1985, *AJ*, 90, 708
- Kennicutt, R. C. 1998, *ARA&A*, 36, 189
- Kennicutt, R. C., Roettiger, K. A., Keel, W. C., van der Hulst, J. M., & Hummel, E. 1987, *AJ*, 93, 1011
- Kleinmann, S. G., & Hall, D. N. B. 1986, *ApJS*, 62, 501
- Kudritzki, R. P. 1998, in *Stellar Astrophysics for the Local Group*, ed. A. Aparicio, A. Herrero, & F. Sanchez (Cambridge: Cambridge Univ. Press), 149
- Lançon, A., & Rocca-Volmerange, B. 1992, *A&AS*, 96, 593
- Larkin, J. E., Armus, L., Knop, R. A., Soifer, B. T., & Matthews, K. 1998, *ApJS*, 114, 59
- Leitherer, Claus, et al. 1999, *ApJS*, 123, 3 (Starburst99)
- Mannucci, F., Basile, F., Poggianti, B. M., Cimatti, A., Daddi, E., Pozzetti, L., & Vanzl, L. 2001, *MNRAS*, 326, 745
- Maoz, D., Ho, L. C., & Sternberg, A. 2001, *ApJ*, 554, L139
- Meyer, M. R., Edwards, S., Hinkle, K. H., & Strom, S. E. 1998, *ApJ*, 508, 397
- Mihos, J. C., & Hernquist, L. 1994, *ApJ*, 425, L13

- Mihos, J. C., & Hernquist, L. 1996, *ApJ*, 464, 641
- Morel, T., Doyon, R., & St-Louis, N. 2002, *MNRAS*, 329, 398
- Mouri, H. 1994, *ApJ*, 427, 777
- Murphy, T. W., Soifer, B. T., Matthews, K., Kiger, J. R., & Armus, L. 1999, *ApJ*, 525, 85
- Murphy, T. W., Soifer, B. T., Matthews, K., Armus, L., & Kiger, J. R. 2001, *AJ*, 121, 97
- Noguchi, M. 1988, *A&A*, 203, 259
- Oliva, E., Moorwood, A. F. M., & Danziger, I. J. 1989, *A&A*, 214, 307
- Oliva, E., Origlia, L., Maiolino, R., & Moorwood, A. F. M. 1995, *A&A*, 301, 55
- Oliva, E., Origlia, L., Maiolino, R., & Moorwood, A. F. M. 1999, *A&A*, 350, 9
- Origlia, L., Moorwood, A. F. M., & Oliva, E. 1993, *A&A*, 280, 536
- Origlia, L., & Oliva, E. 2000, *A&A*, 357, 61
- Origlia, L., Leitherer, C., Aloisi, A., Greggio, L., & Tosi, M. 2001, *AJ*, 122, 815
- Rayner, J. T., Toomey, D. W., Onaka, P. M., Denault, A. J., Stahlberger, W. E., Vacca, W. D., Cushing, M. C., & Wang S. 2003, *PASP*, in press
- Reunanen, J., Kotilainen, J. K., & Prieto, M. A. 2002, *MNRAS*, 331, 154
- Rodriguez Espinosa, J. M., Rudy, R. J., & Jones, B. 1987, *ApJ*, 312, 555
- Roussel, H., et al. 2001, *A&A*, 369, 473
- Rudnick, G., Rix, H.-W., & Kennicutt, R. C. 2000, *ApJ*, 538, 569
- Sandage, A., & Bedke, J. 1994, *Canegie Atlas of Galaxies* (Washington: Carnegie Institution)
- Sandage, A., & Tammann, G. A. 1987, *A Revised Shapley-Ames Catalog of Bright Galaxies* 2nd ed. (Washington: Carnegie Institution)
- Shields, J. C. 1992, *ApJ*, 399, L27
- Sosa-Brito, R. M., Tacconi-Garman, L. E., & Lehnert, M. D. 2001, *ApJS*, 136, 61
- Terlevich, R., & Melnick, J. 1985, *MNRAS*, 213, 841
- van der Werf, P. P., Genzel, R., Krabbe, A., Blietz, M., Lutz, D., Drapatz, S., Ward, M. J., & Forb, D. A. 1993, *ApJ*, 405, 522
- van Moorsel, G. A. 1983, *A&AS*, 54, 19
- Vanzi, L., Alonso-Herrero, A., & Rieke, G. H. 1998, *ApJ*, 504, 93
- Vanzi, L., & Rieke, G. H. 1997, *ApJ*, 479, 694
- Wada, K., & Habe, A. 1992, *MNRAS*, 258, 82
- Wada, K., & Habe, A. 1995, *MNRAS*, 277, 433
- Wallace, L., & Hinkle, K. 1997, *ApJS*, 111, 445

Wallace, L., & Livingston, W. 1992, An Atlas of a Dark Sunspot Umbral Spectrum from 1970 to 8640 cm^{-1} (1.16 to $5.1\ \mu\text{m}$), NSO Technical Report #92-001 (Tucson: National Solar Observatory)

Wright, G. S., Joseph, R. D., Robertson, N. A., James, P. A., & Meikle, W. P. S. 1988, MNRAS, 233, 1

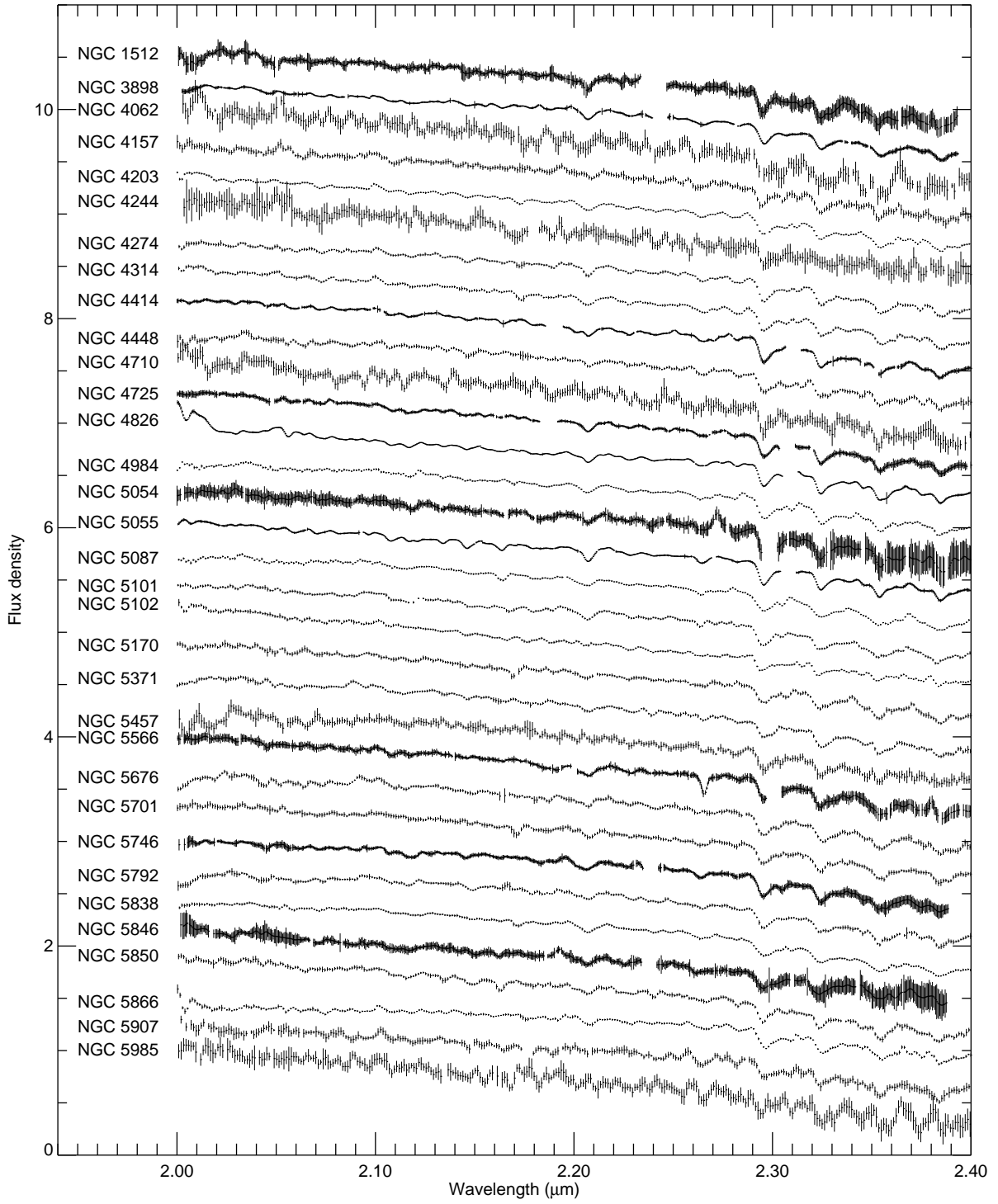


Fig. 1.— The K-band spectra of the 33 quiescent galaxies. The flux density units are arbitrary but are in terms of flux per unit wavelength. An artificial offset has been applied to display all the spectra in this plot.

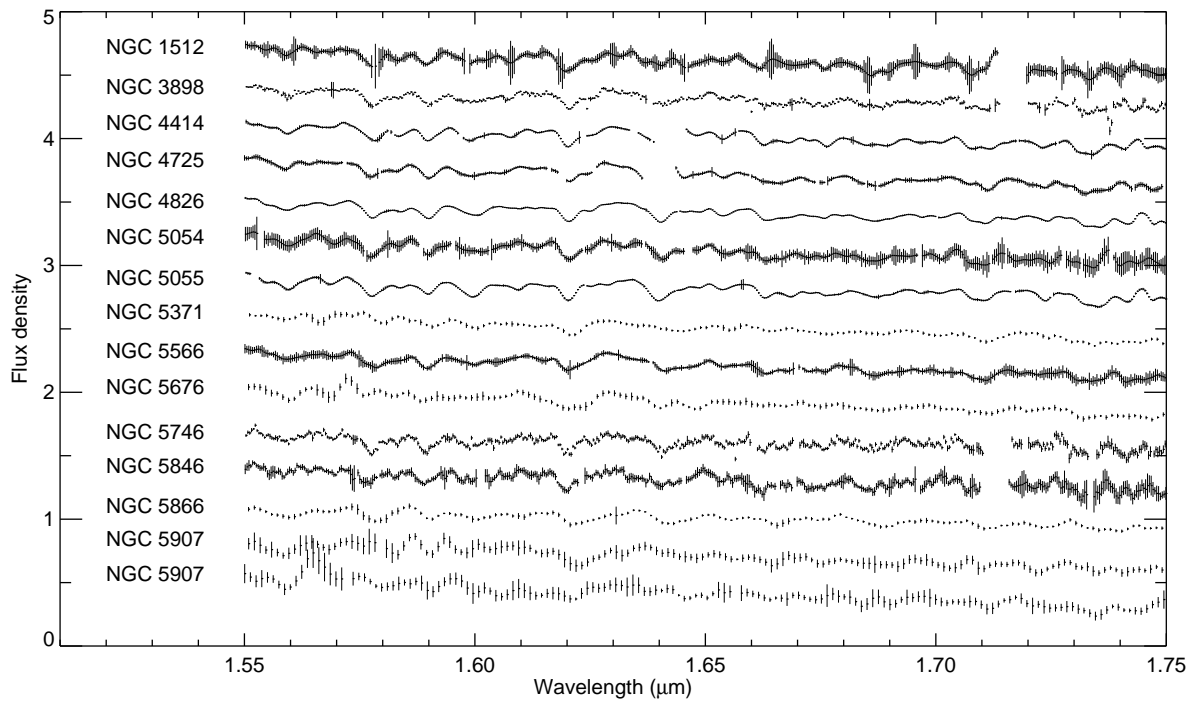


Fig. 2.— The 15 available H-band spectra of quiescent galaxies. The flux density units are arbitrary but are in terms of flux per unit wavelength. An artificial offset has been applied to display all the spectra in this plot.

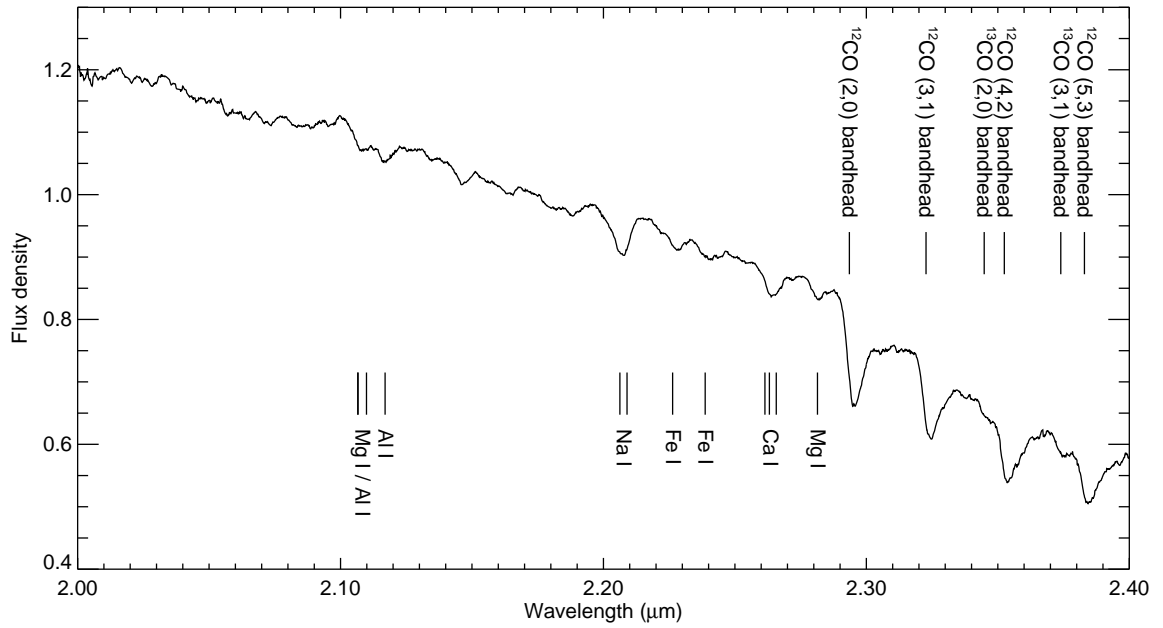


Fig. 3.— The composite quiescent spectrum in the K-band. The flux density units are arbitrary but are in terms of flux per unit wavelength. The median value of the flux density in the region between 2.10 and 2.28 μm has been normalized to 1. Strong absorption features have been marked.

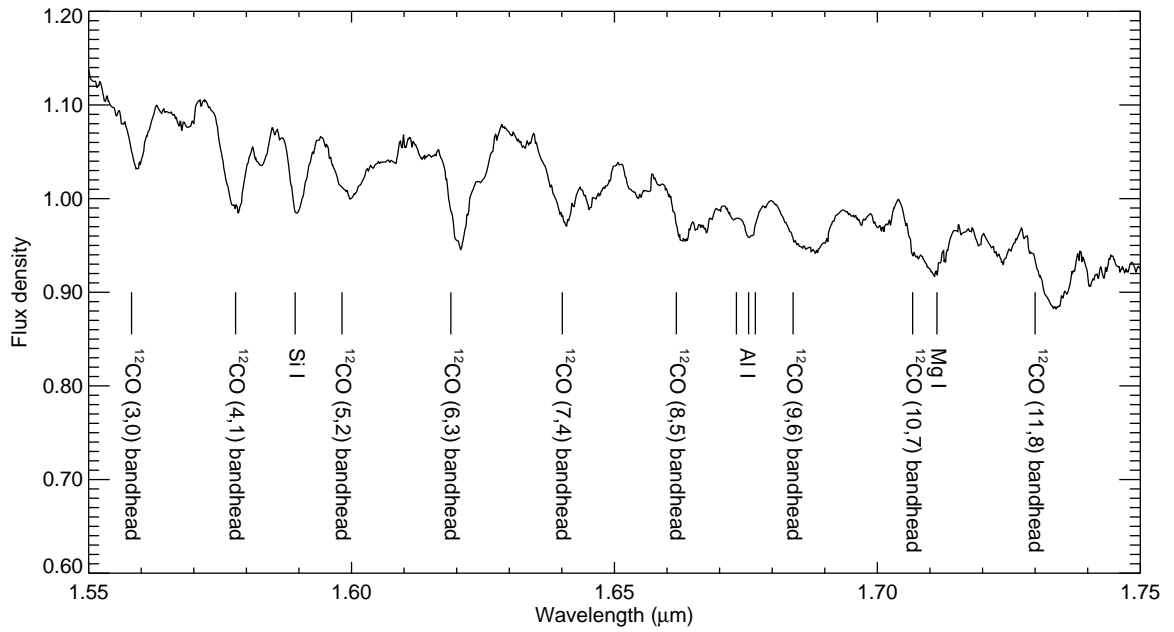


Fig. 4.— The composite quiescent spectrum in the H-band. The flux density units are arbitrary but are in terms of flux per unit wavelength. The median value of the flux density in the region between 1.55 and 1.75 μm has been normalized to 1. Strong absorption features have been marked.

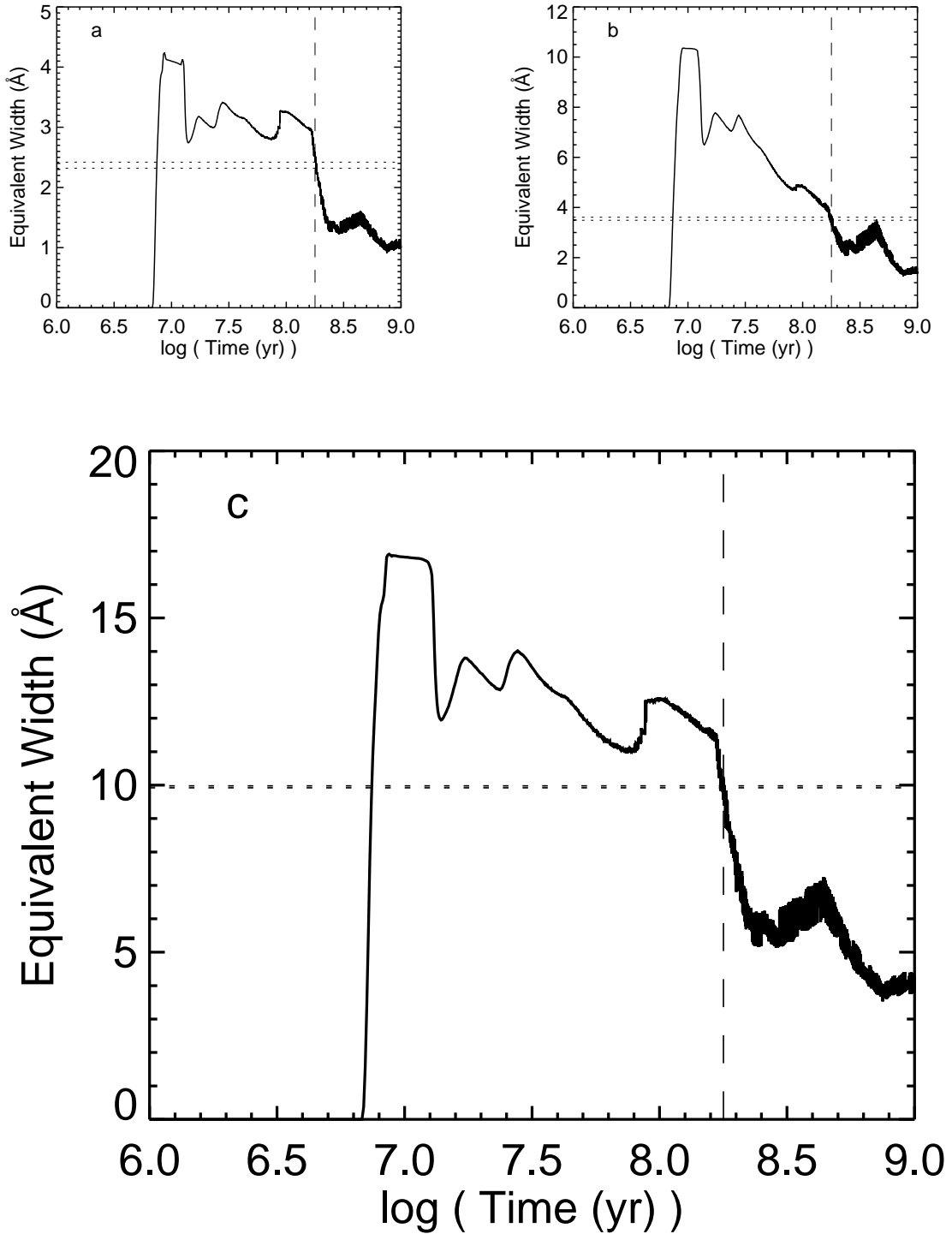


Fig. 5.— Plots of (a) the Si I 1.59 μm equivalent width, (b) the CO 6-3 1.62 μm equivalent width, and (c) the CO 2-0 2.29 μm equivalent width after an instantaneous burst of star formation that produces an IMF with a slope of 2.35 and an upper mass cutoff of $100 M_{\odot}$, as determined using Starburst99. The 1σ errors in the measured equivalent widths for the composite quiescent spectrum are superimposed as dotted horizontal lines. The dashed vertical lines shows where the χ^2 value is at a minimum.

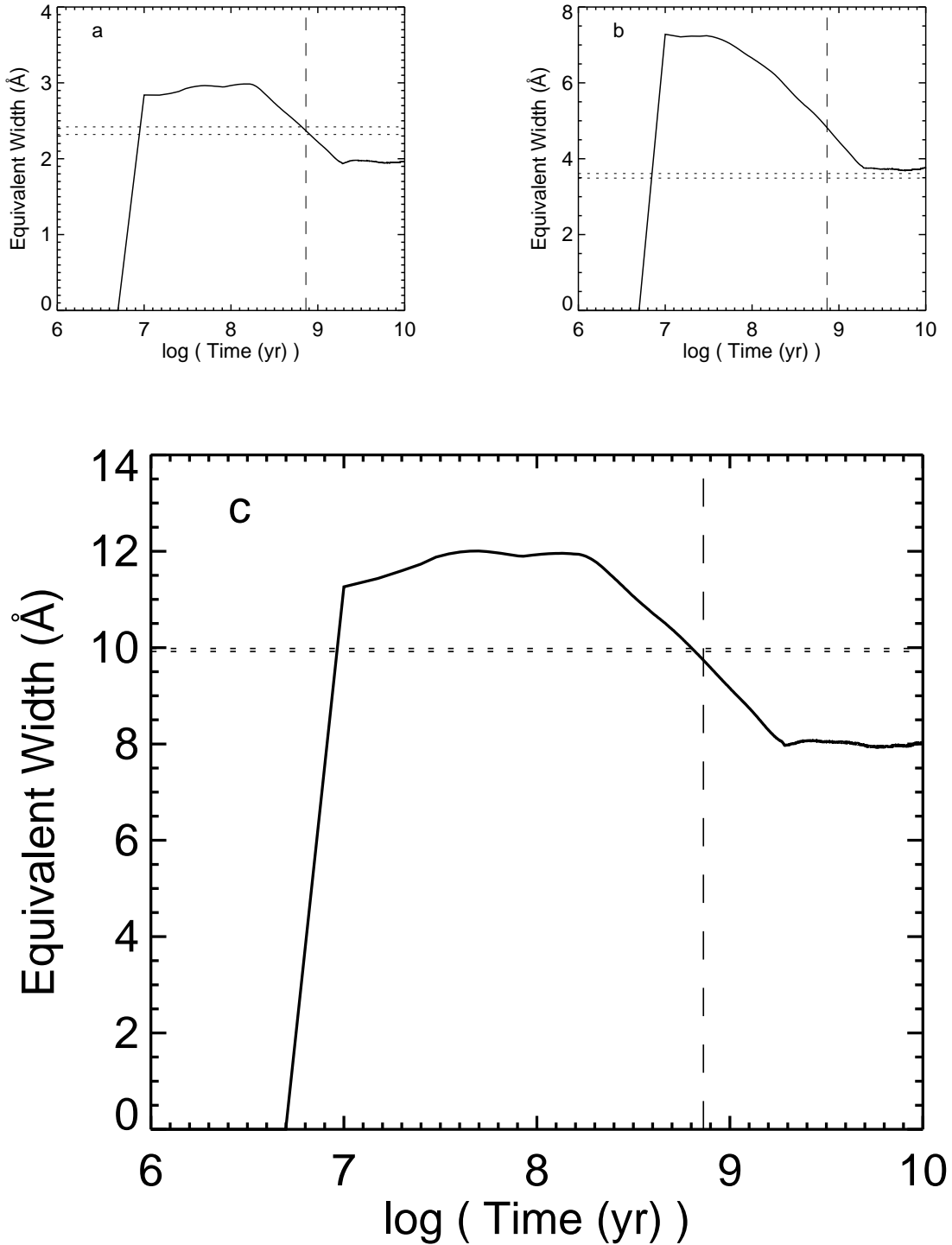


Fig. 6.— Plots of (a) the Si I 1.59 μm equivalent width, (b) the CO 6-3 1.62 μm equivalent width, and (c) the CO 2-0 2.29 μm equivalent width after the onset of continuous star formation that produces an IMF with a slope of 2.35 and an upper mass cutoff of 100 M_{\odot} , as determined using Starburst99. The 1σ errors in the measured equivalent widths for the composite quiescent spectrum are superimposed as dotted horizontal lines. The dashed vertical lines shows where the χ^2 value is at a minimum.

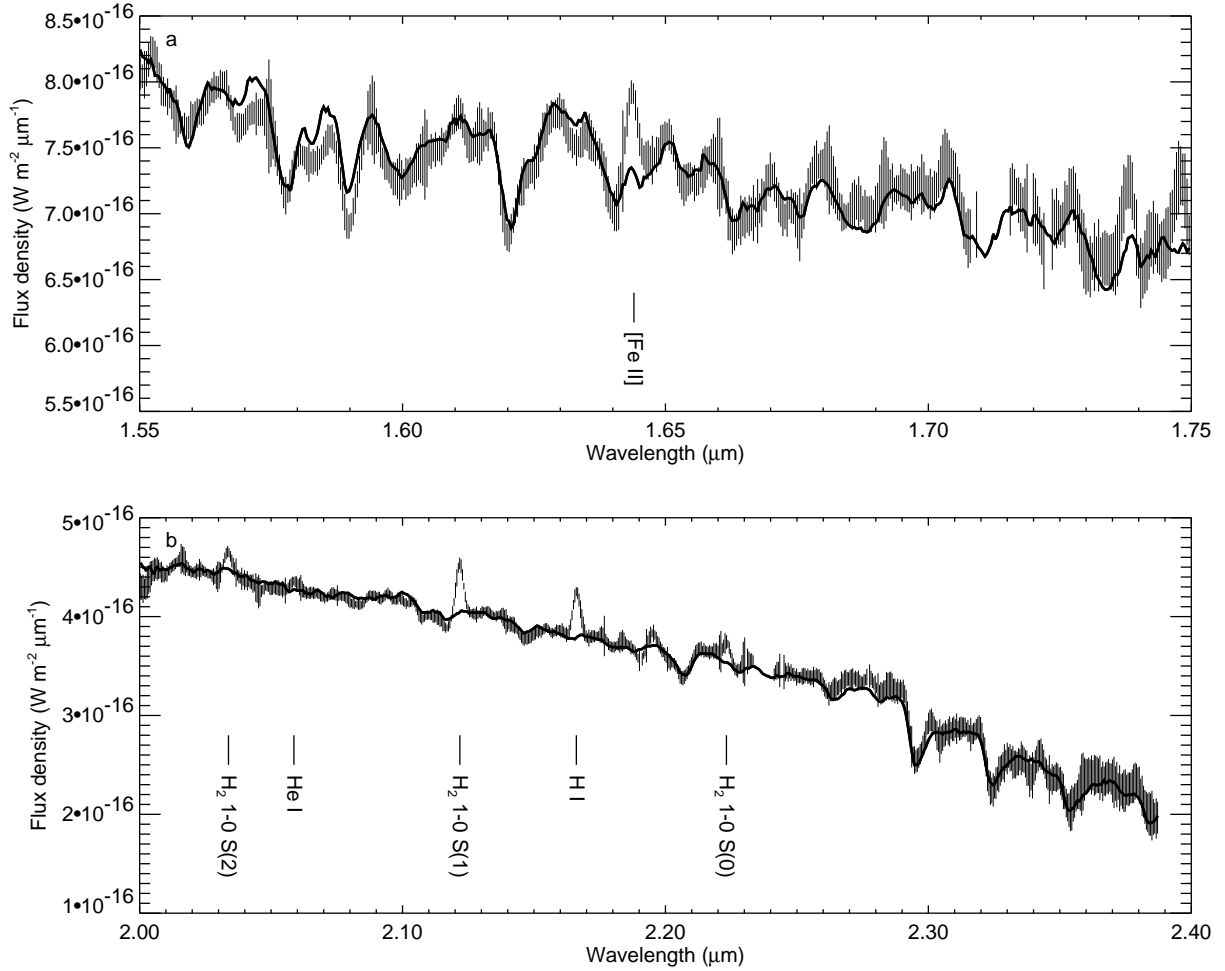


Fig. 7.— The (a) H-band and (b) K-band spectra of NGC 289 (plotted as vertical error bars) in the rest frame with the composite quiescent spectrum overlaid as a thick black line. Emission lines of interest are indicated in the plot. All following non-quiescent spectra will be plotted in the same format. Note the strong Fe II emission at $1.64 \mu\text{m}$, the strong H_2 emission at $2.12 \mu\text{m}$ and the strong Brackett- γ emission at $2.17 \mu\text{m}$.

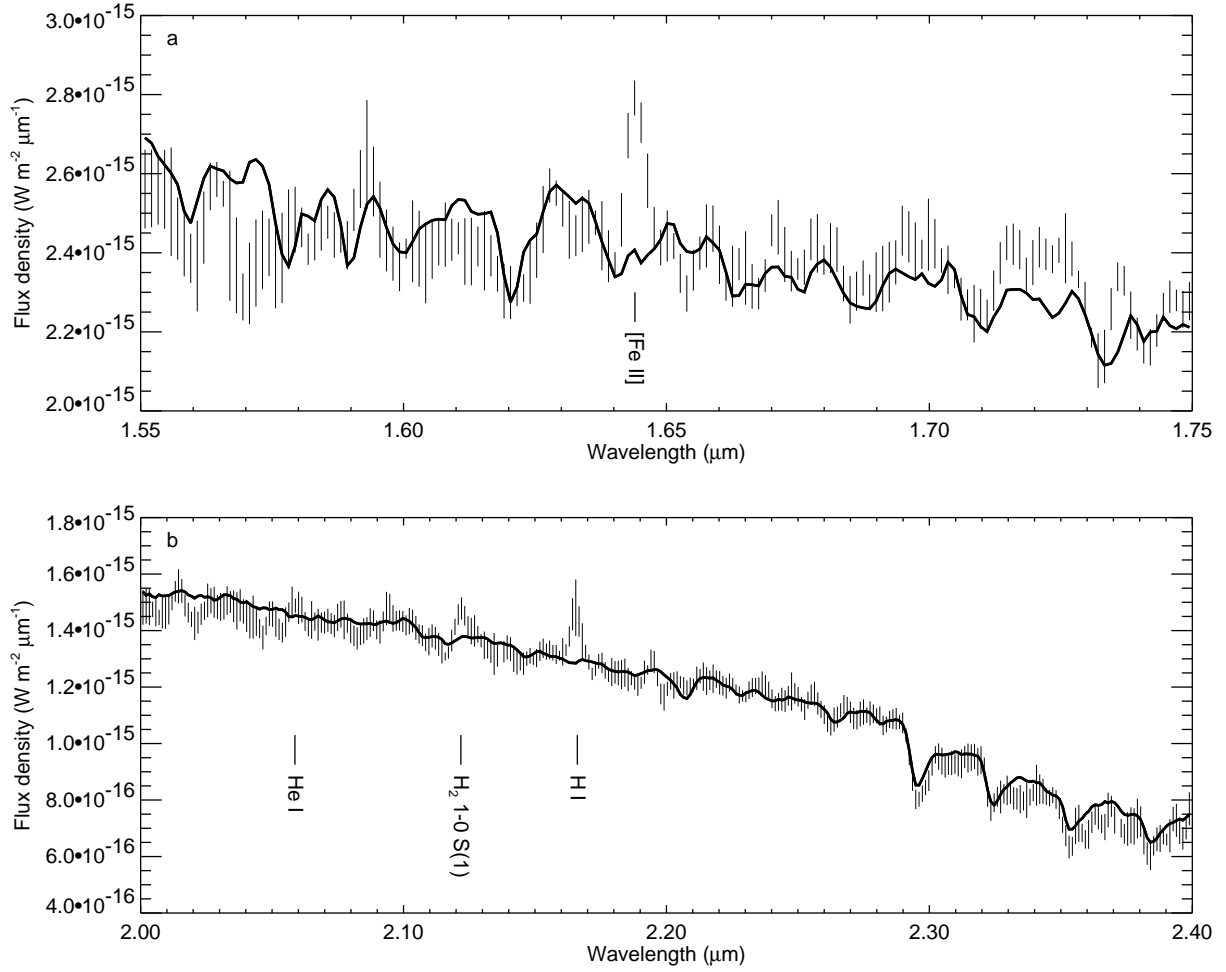


Fig. 8.— The (a) H-band and (b) K-band spectra of NGC 5713. Again, note the strong Fe II, H_2 , and Brackett- γ emission.

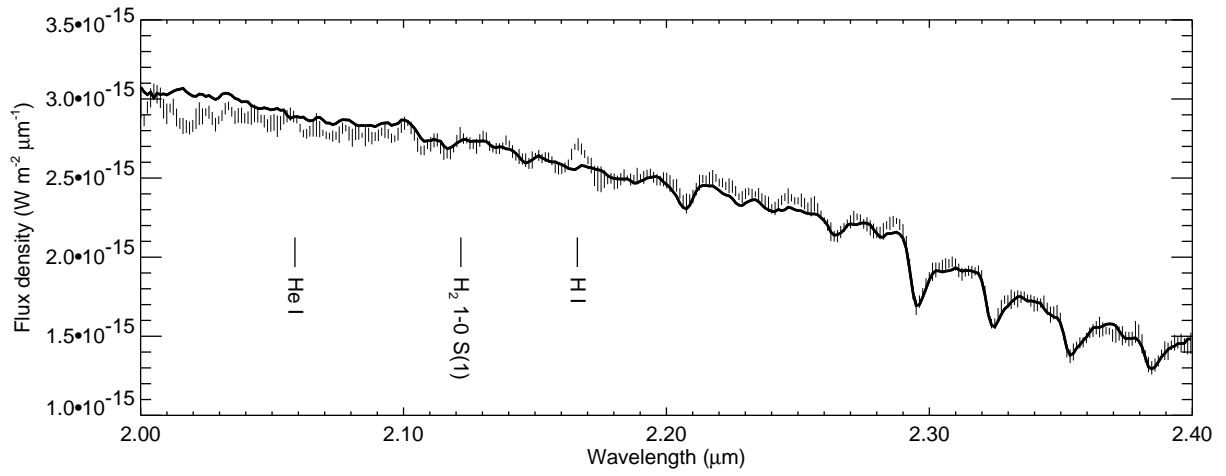


Fig. 9.— The K-band spectrum of NGC 4088. Only Brackett- γ is strongly detected. (Deviation of the spectrum from the composite quiescent spectrum at wavelengths shorter than 2.10 μm may be a result of the relatively high atmospheric variability in that part of the waveband.)

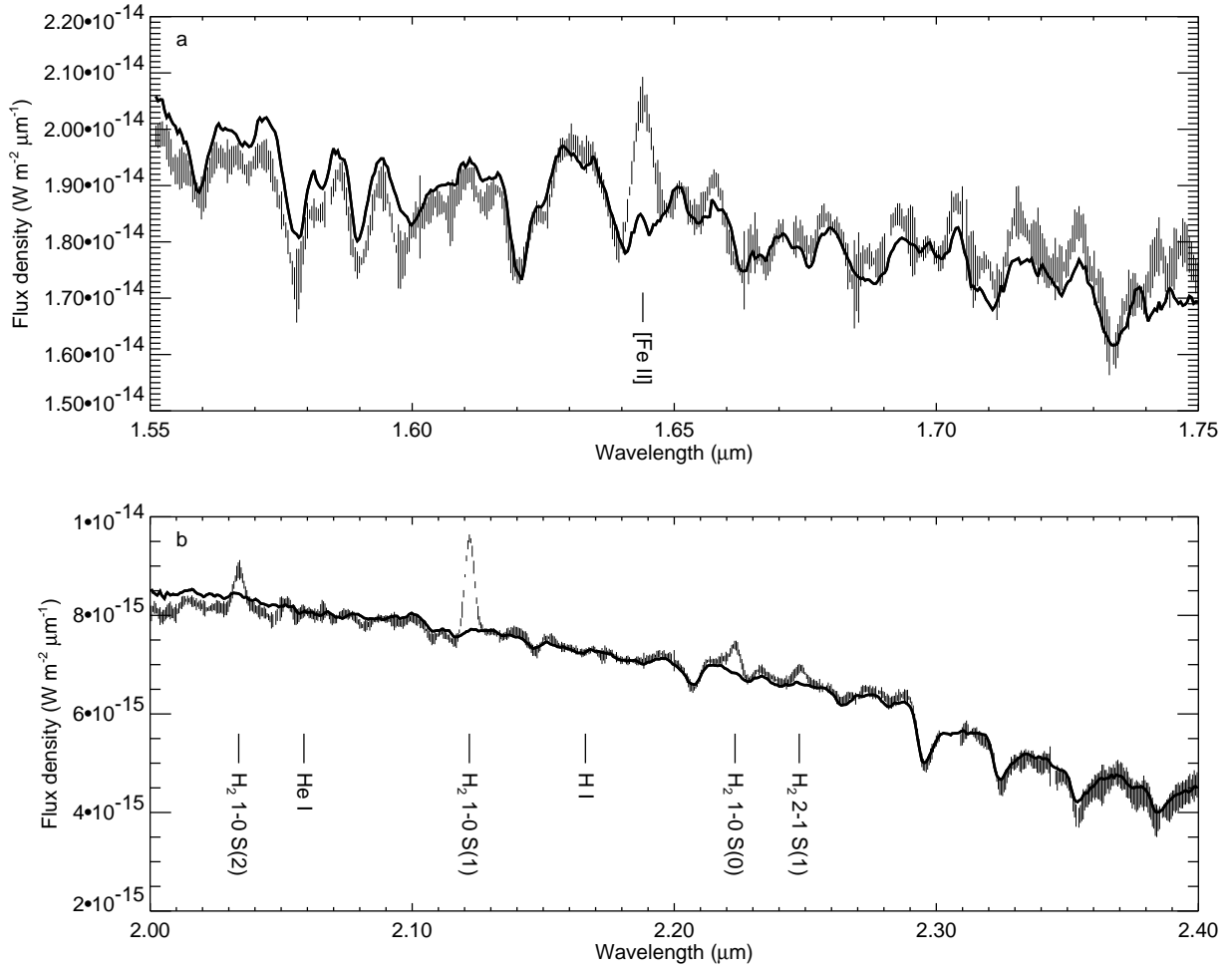


Fig. 10.— The (a) H-band and (b) K-band spectra of NGC 5005. A combination of the composite quiescent spectrum and a power-law continuum have been overlaid as a solid line. Note the strong shock excitation lines but the absence of Brackett- γ emission.

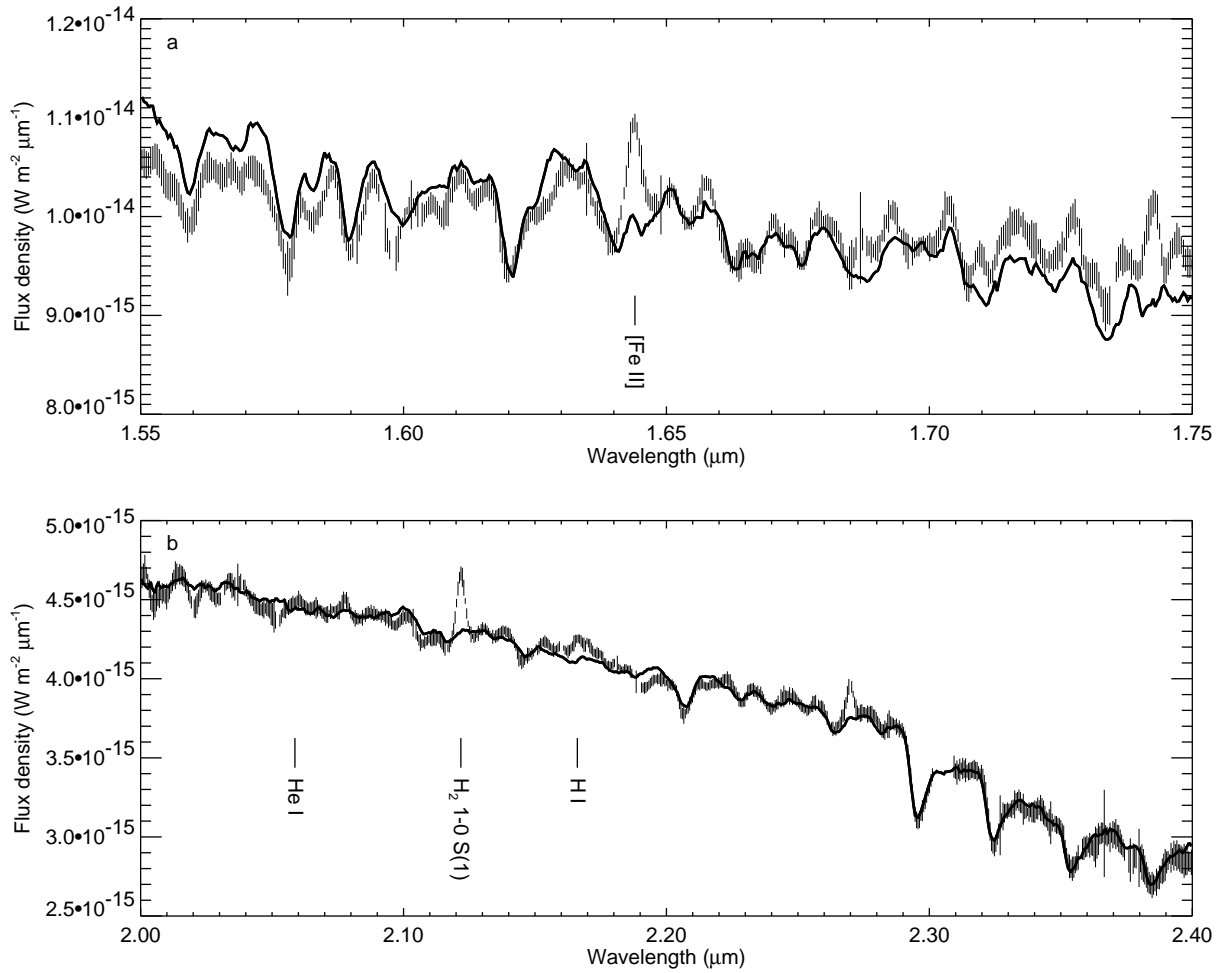


Fig. 11.— The (a) H-band and (b) K-band spectra of NGC 5033. As with NGC 5005, a combination of the composite quiescent spectrum and a power law have been overlaid as a solid line in the K-band plot. The strong shock excitation lines are the most obvious features in this spectrum, but a broad yet weak Brackett- γ feature is present.

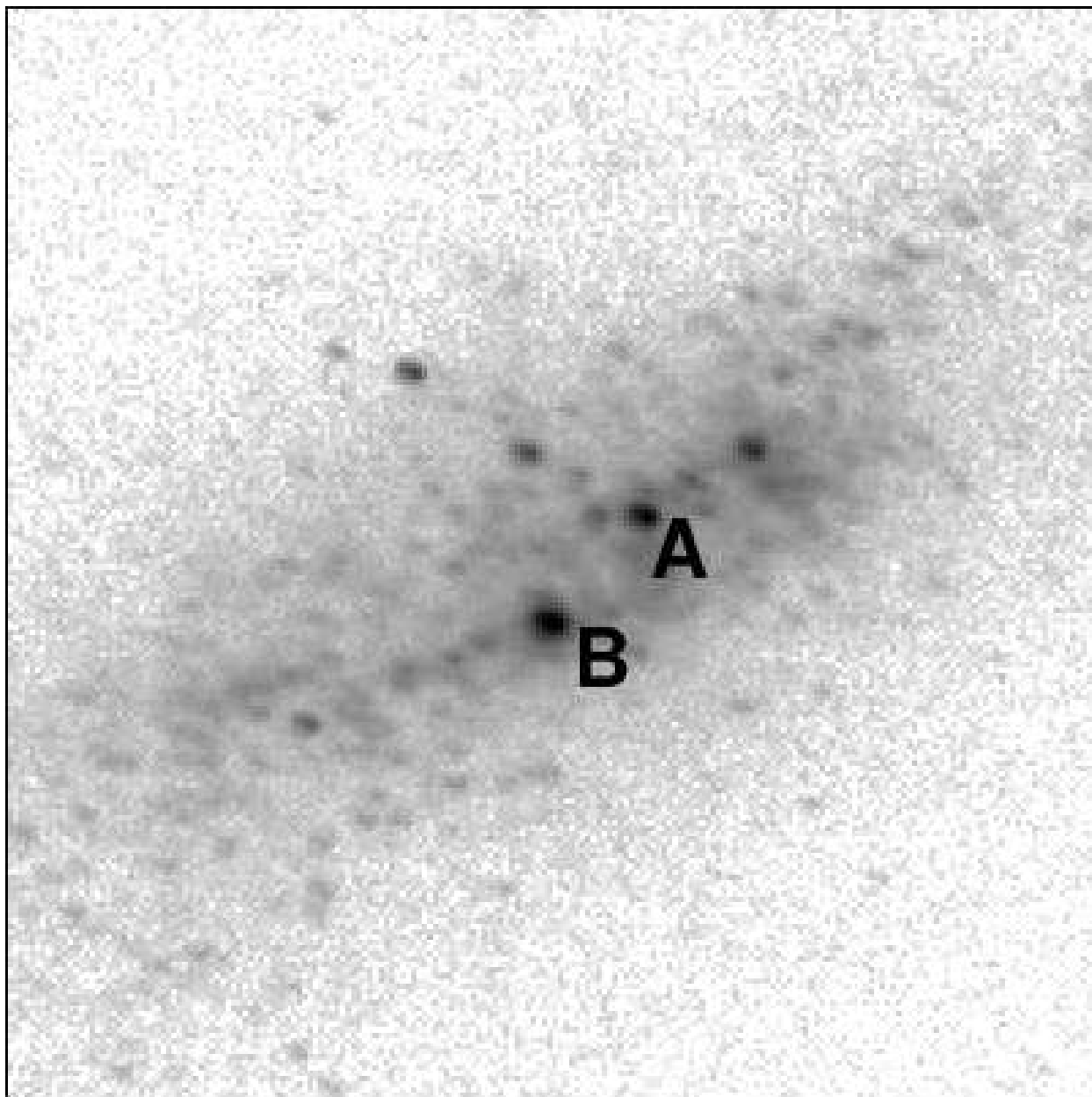


Fig. 12.— A K-band image of the inner 60'' of NGC 1569, with the A and B clusters identified in the image. North is up and east is left.

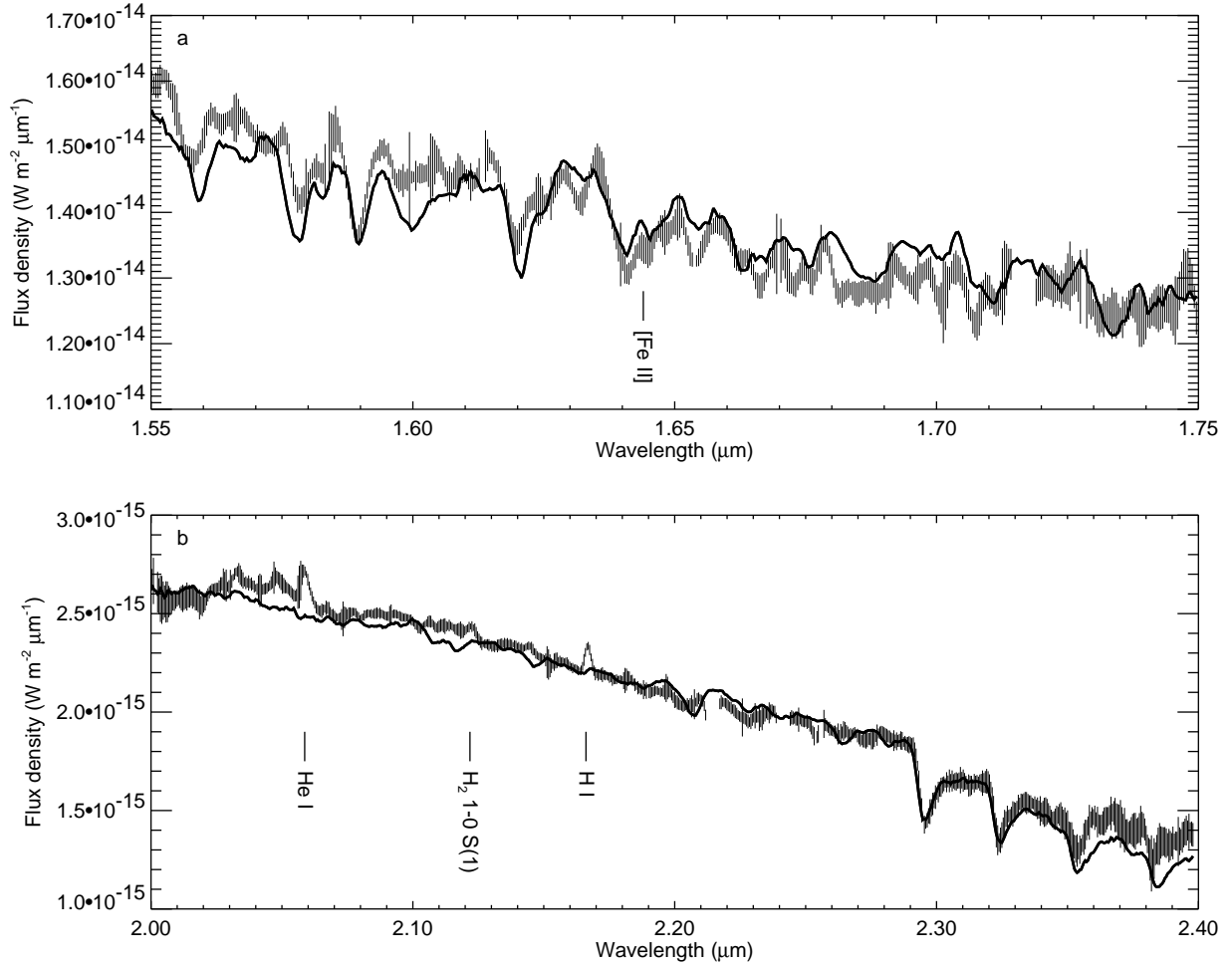


Fig. 13.— The (a) H-band and (b) K-band spectra of cluster A in NGC 1569. Note not only the presence of He I and Brackett- γ emission lines but also the relatively weak metal lines in the K-band.

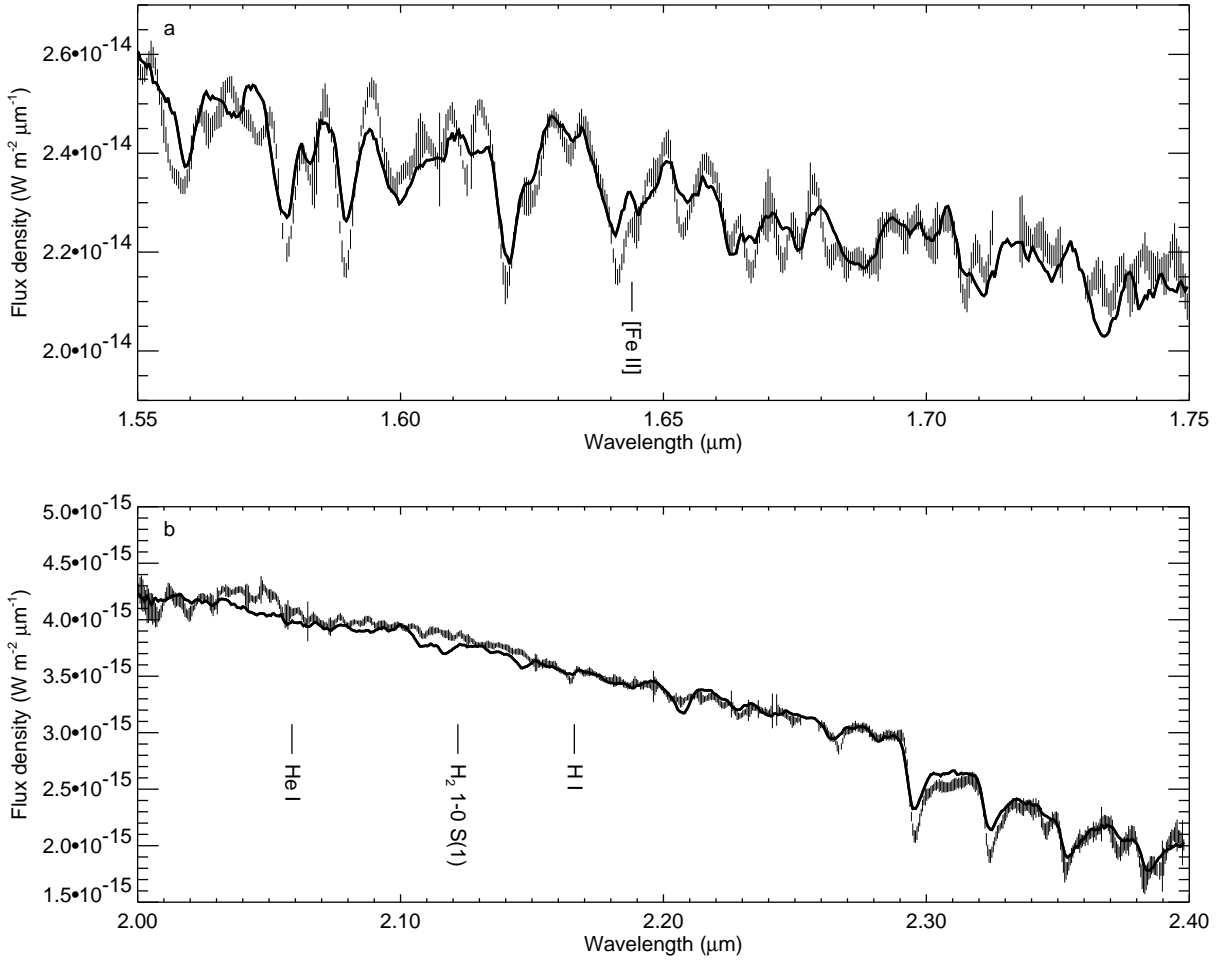


Fig. 14.— The (a) H-band and (b) K-band spectra of cluster B in NGC 1569. In contrast to the spectra for cluster A, these spectra lack the He I and Brackett- γ emission lines. However, they do include the same relatively shallow metal absorption features. They also feature deeper CO features than the overlaid composite quiescent spectrum, which indicates that the continuum is dominated by red giants younger than 180 Myr.

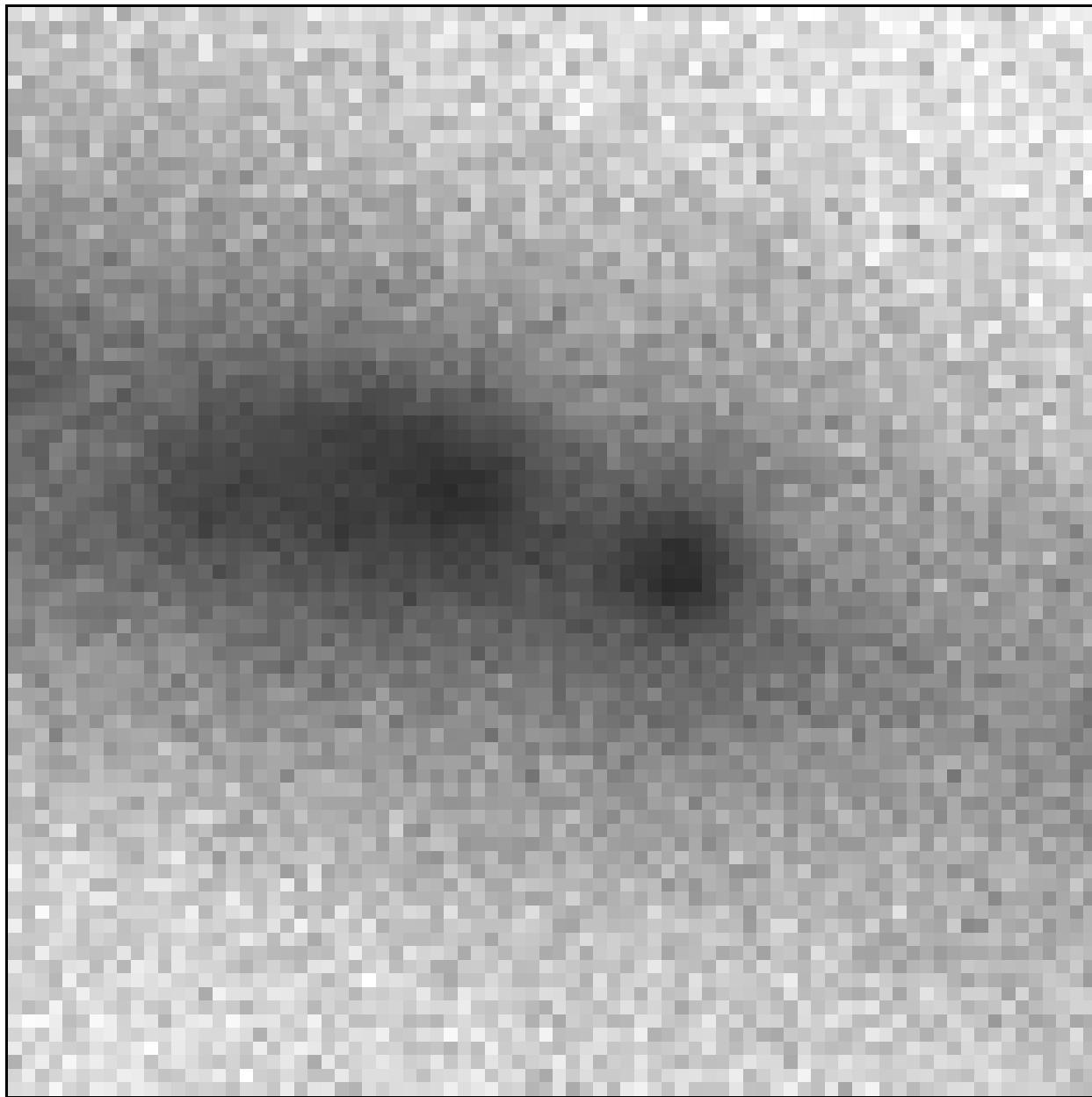


Fig. 15.— A K-band image of the inner 15'' of NGC 3556. This corresponds to a physical size of 1 kpc. North is up and east is left. The east and west nuclear regions are both evident in this image.

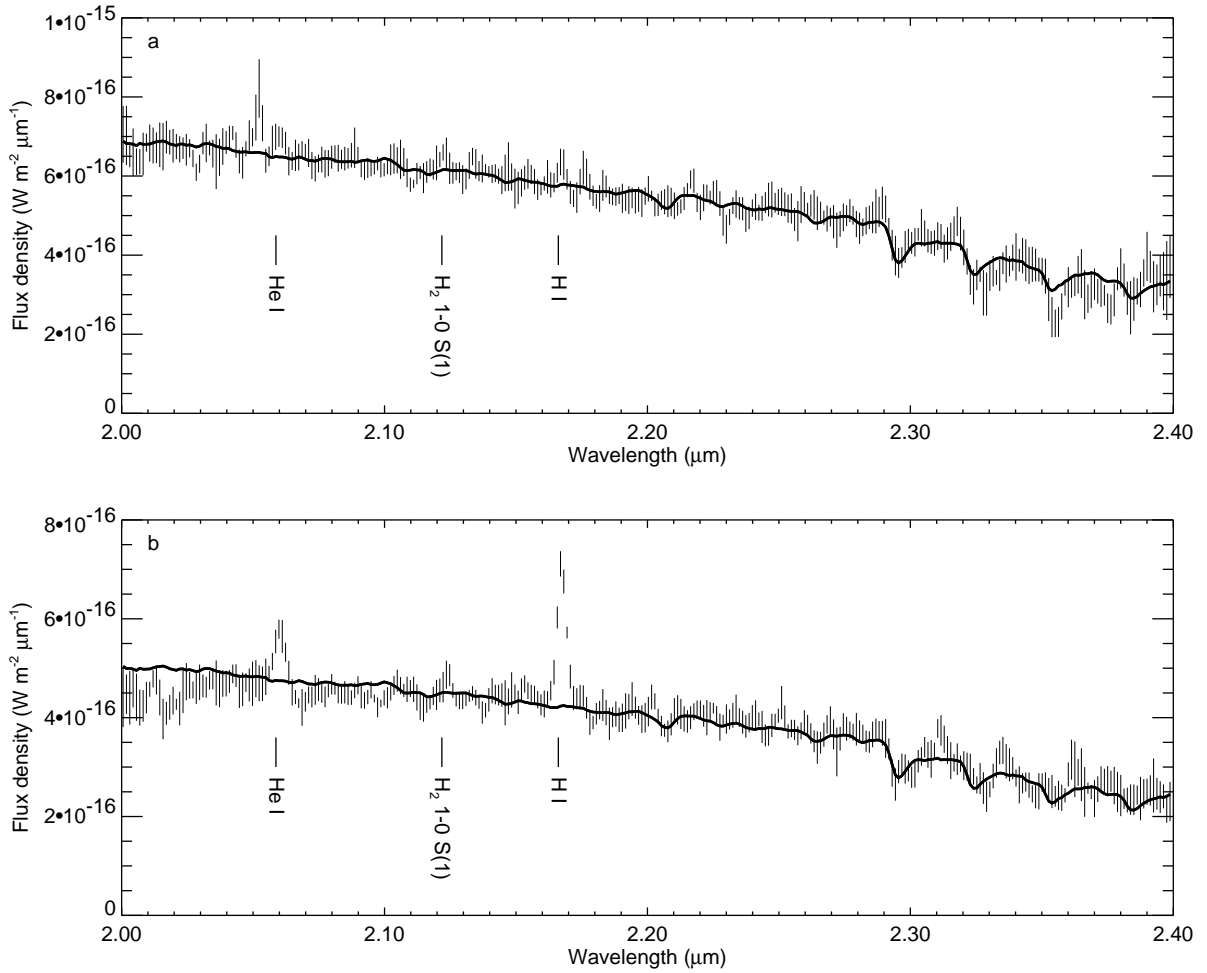


Fig. 16.— The K-band spectra of (a) the east nuclear region and (b) the west nuclear region of NGC 3556. Brackett- γ and He I lines are present in the spectrum for the west nuclear region but not the east nuclear region. (The narrow spike near 2.05 μm in the spectrum of the east nuclear region appears to be artificial.)

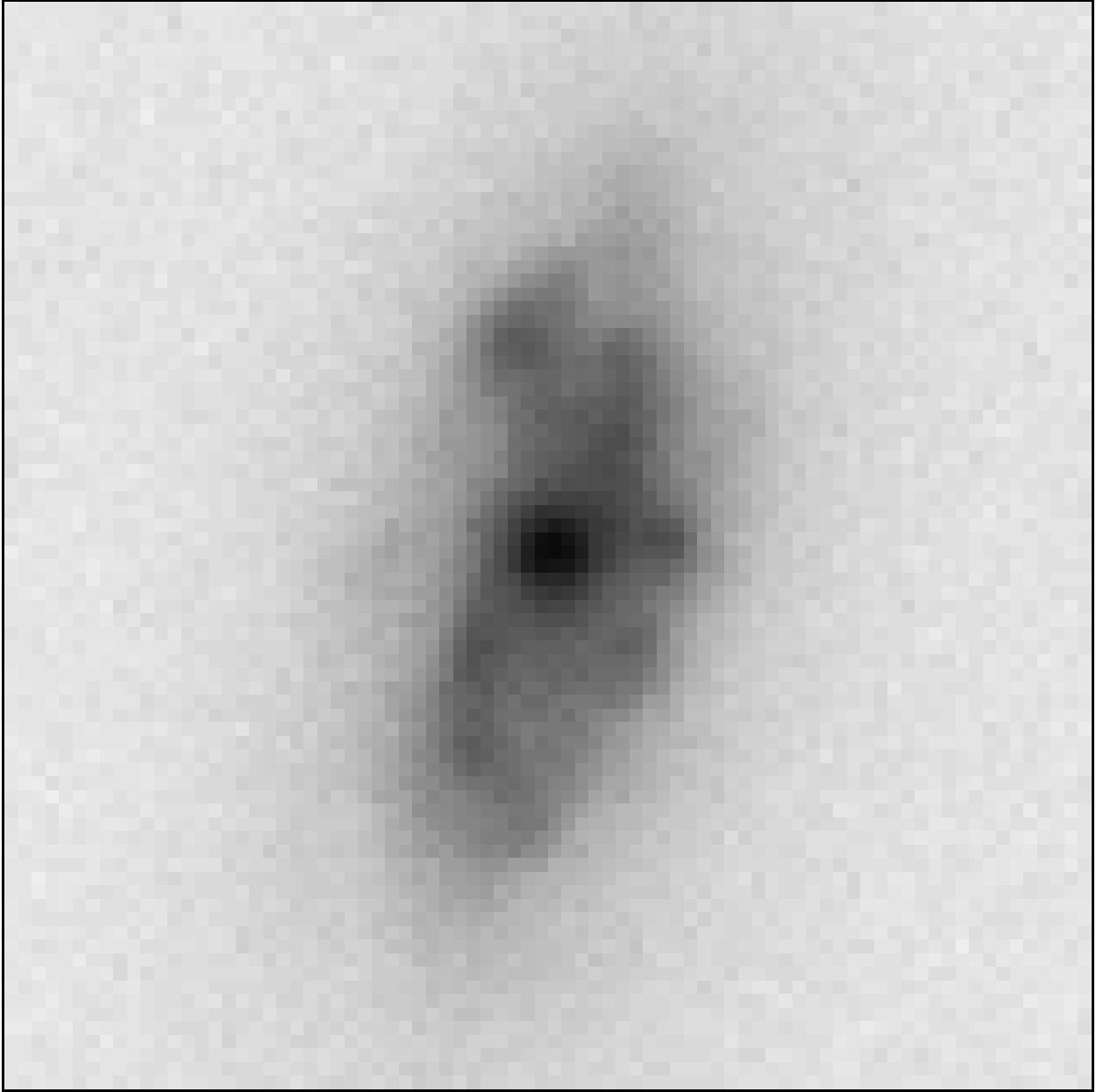


Fig. 17.— A K-band image of the inner 15'' of NGC 4100. This corresponds to a physical size of 1.2 kpc. North is up and east is left. Note the knotted structure of this galaxy's nucleus.

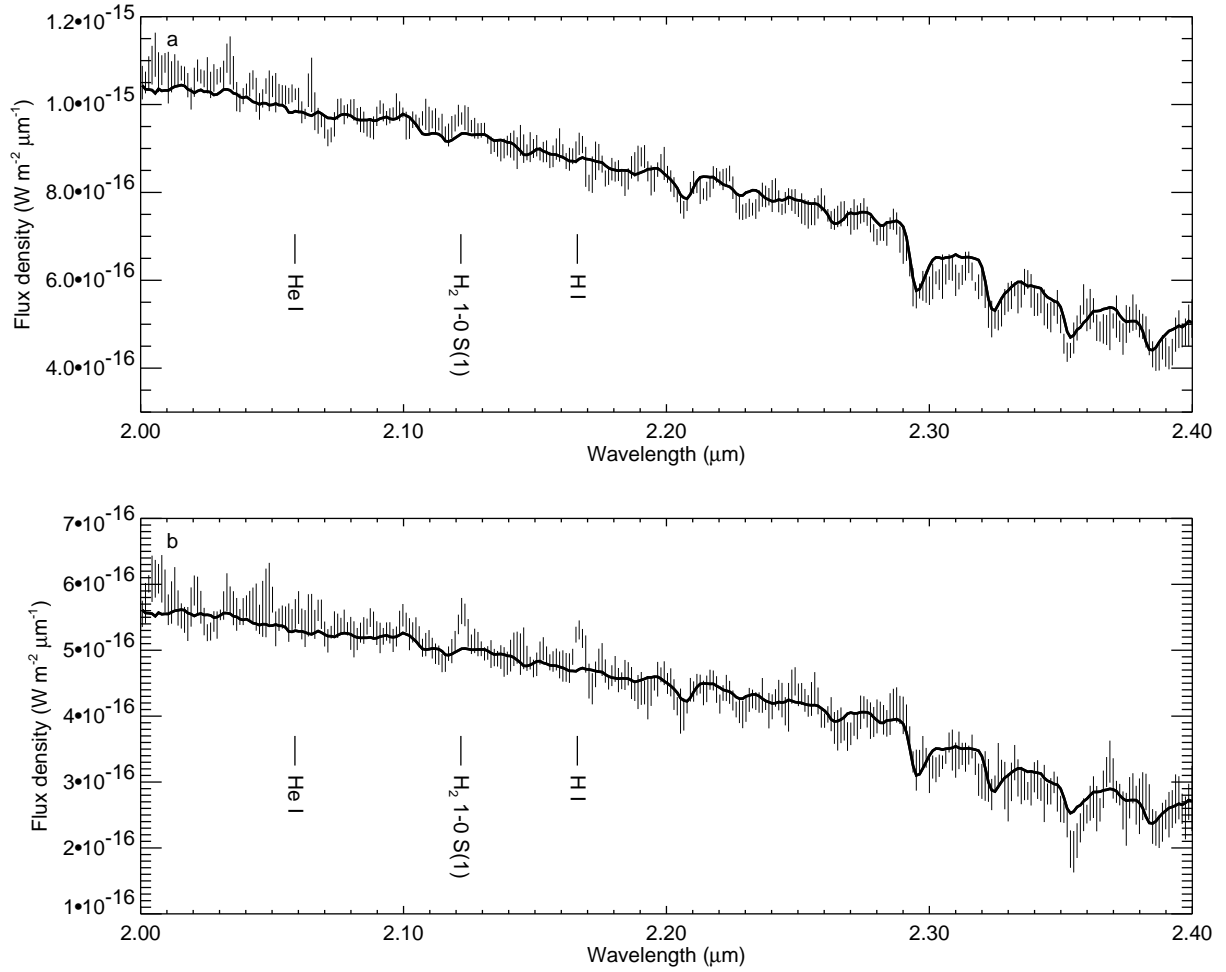


Fig. 18.— The K-band spectra of (a) the nucleus and (b) the region 1.2'' south of the nucleus in NGC 4100. The nucleus produces a quiescent spectrum, but the region just to the south produces both photoionization and shock excitation lines.

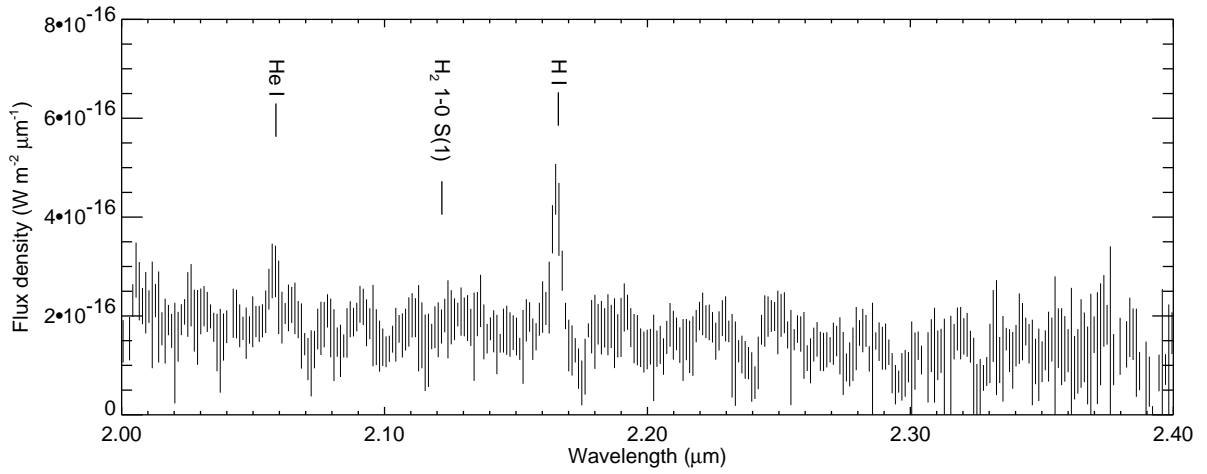


Fig. 19.— The K-band spectrum of the northern knot of NGC 5676. Note the weak continuum and very strong Brackett- γ and He I lines.

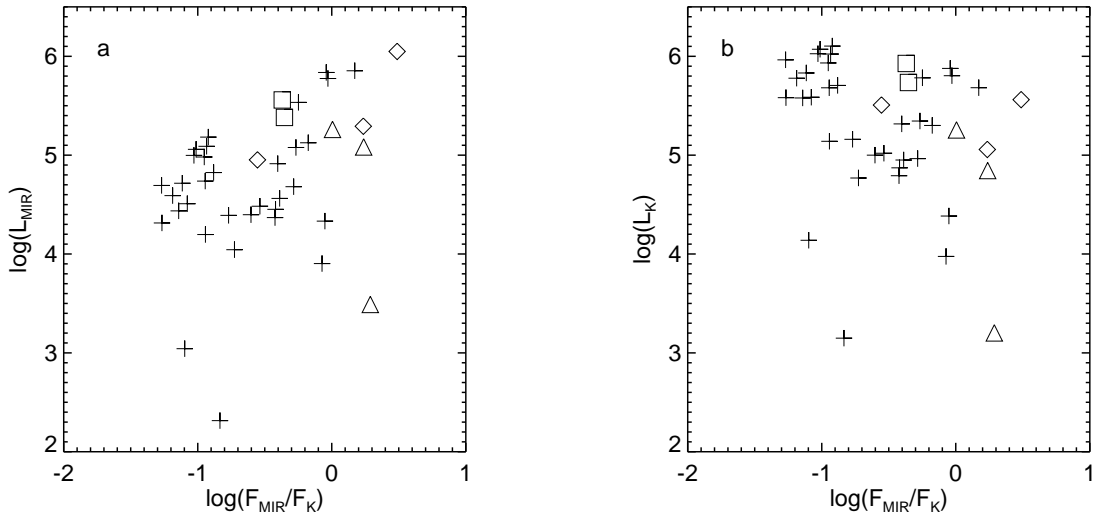


Fig. 20.— The (a) mid-infrared luminosities and (b) K-band luminosities plotted against ratio of the mid-infrared to K-band fluxes. The luminosities are in units of L_{\odot} . The crosses represent quiescent objects, while the open symbols represent non-quiescent objects. The triangles indicate non-quiescent galaxies with only recombination line emission. The diamonds indicate galaxies with recombination and shock excitation line emission. The squares indicate galaxies with only shock excitation line emission.

Table 1. Morphology, Distance, and Nuclear Activity Data for the Sample

Galaxy	Morphological Type ^a	Distance (Mpc) ^b	Nuclear Activity ^c
NGC 289	SB(rs)bc	19.4	...
NGC 1512	SB(r)a	9.5	...
NGC 1569	IBm	1.6	H
NGC 3556	SB(s)cd	14.1	H
NGC 3898	SA(s)ab	21.9	T2
NGC 4088	SAB(rs)bc	17.0	H
NGC 4096	SAB(rs)c	8.8	H
NGC 4100	PSA(rs)bc	17.0	H
NGC 4157	SAB(s)b	17.0	H
NGC 4203	SAB0	9.7	L1.9
NGC 4244	SA(s)cd	3.1	H
NGC 4274	RSB(r)ab	9.7	H
NGC 4314	SB(rs)a	9.7	L2
NGC 4414	SA(rs)c	9.7	T2:
NGC 4448	SB(r)ab	9.7	H
NGC 4710	SA(r)0	16.8	H
NGC 4725	SAB(r)ab pec	12.4	S2:
NGC 4826	RSA(rs)ab	4.1	T2
NGC 4984	RSAB(rs)0	21.3	...
NGC 5005	SAB(rs)bc	21.3	L1.9
NGC 5033	SA(s)c	18.7	S1.5
NGC 5054	SA(s)bc	27.3	...
NGC 5055	SA(rs)bc	7.2	T2
NGC 5087	SA0	27.8	...
NGC 5101	RSB(rs)0/a	27.4	...
NGC 5102	SA0	3.5	...
NGC 5170	SA(s)c	24.0	...
NGC 5371	SAB(rs)bc	37.8	L2
NGC 5457	SAB(rs)cd	5.4	H
NGC 5566	SB(r)ab	26.4	L2
NGC 5676	SA(rs)bc	34.5	H
NGC 5701	RSB(rs)0/a	26.1	T2:
NGC 5713	SAB(rs)bc pec	30.4	...
NGC 5746	SAB(rs)b	29.4	T2
NGC 5792	SB(rs)b	30.6	...
NGC 5838	SA0	28.5	T2::
NGC 5846	E0	28.5	T2:
NGC 5850	SB(r)b	28.5	L2

Table 1—Continued

Galaxy	Morphological Type ^a	Distance (Mpc) ^b	Nuclear Activity ^c
NGC 5866	SA0	15.3	T2
NGC 5907	SA(s)c	14.9	H:
NGC 5985	SAB(r)b	39.2	L2

^aAs defined in RC3.

^bDesignations as given in HFS97b. S = Seyfert. L = LINER. H = HII nucleus. T = Transitional. The number indicates the type of AGN activity. Single colons indicate uncertain classifications. Double colons indicate highly uncertain classifications. Note that the classifications are based strictly on optical line ratios and that not all galaxies have been classified.

Table 2. K-Band Observations Information

Target	Date of Observations	Instrument	Total Integration Time (s)	Spectroscopic Standard Types
NGC 289	19 Sep 2000	SPEX	2400	A0V, G2Ib
NGC 1512	17 Sep 2000	SPEX	1800	A0V
NGC 1569	16 Sep 2000	SPEX	2400	A0V, G2V
NGC 3556	08 May 2001	CGS4	960	G2V
NGC 3898	04 Apr 2001	SPEX	1200	A0V, G5
NGC 4088	08 May 2001	CGS4	960	G2V
NGC 4096	10 May 2001	CGS4	960	G5V
NGC 4100	09 May 2001	CGS4	960	G5V
NGC 4157	09 May 2001	CGS4	960	G5V
NGC 4203	07 May 2001	CGS4	960	G5V
NGC 4244	08 May 2001	CGS4	960	G5V
NGC 4274	07 May 2001	CGS4	960	G5V
NGC 4314	07 May 2001	CGS4	960	G5V
NGC 4414	07 Jun 2000	SPEX	1200	A0V
NGC 4448	07 May 2001	CGS4	960	G5V
NGC 4710	10 May 2001	CGS4	960	G2V
NGC 4725	07 Jun 2000	SPEX	1200	A0V
NGC 4826	05 Jun 2000	SPEX	2160	A0
NGC 4984	10 May 2001	CGS4	960	G6V
NGC 5005	05 Jun 2000	SPEX	720	A0V
NGC 5033	06 Jun 2000	SPEX	1200	A0V
NGC 5054	08 Jun 2000	SPEX	1200	A0V
NGC 5055	06 Jun 2000	SPEX	1200	A0V
NGC 5087	10 May 2001	CGS4	960	G6V
NGC 5101	08 May 2001	CGS4	960	G2V
NGC 5102	09 May 2001	CGS4	960	G3V
NGC 5170	08 May 2001	CGS4	960	G6V
NGC 5371	07 May 2001	CGS4	960	G5V
NGC 5457	09 May 2001	CGS4	960	G5V
NGC 5566	06 Jun 2000	SPEX	720	A0V
NGC 5676	07 May 2001	CGS4	960	G5V
NGC 5701	08 May 2001	CGS4	960	G1V
NGC 5713	07 May 2001	CGS4	960	G1V
NGC 5746	06 Apr 2001	SPEX	1560	A0V, G5
NGC 5792	07 May 2001	CGS4	960	G1V
NGC 5838	08 May 2001	CGS4	960	G1V
NGC 5846	05 Apr 2001	SPEX	1200	A0V, G5

Table 2—Continued

Target	Date of Observations	Instrument	Total Integration Time (s)	Spectroscopic Standard Types
NGC 5850	08 May 2001	CGS4	960	G1V
NGC 5866	07 May 2001	CGS4	960	G5V
NGC 5907	08 May 2001	CGS4	960	G5V
NGC 5985	09 May 2001	CGS4	960	G5V

Table 3. H-Band Observations Information

Target	Date of Observations	Instrument	Total Integration Time (s)	Spectroscopic Standard Types
NGC 289	19 Sep 2000	SPEX	2400	A0V, G2Ib
NGC 1512	17 Sep 2000	SPEX	1800	A0V
NGC 1569	16 Sep 2000	SPEX	2400	A0V, G2V
NGC 3898	04 Apr 2001	SPEX	1200	A0V, G5
NGC 4414	07 Jun 2000	SPEX	1200	A0V
NGC 4725	07 Jun 2000	SPEX	1200	A0V
NGC 4826	05 Jun 2000	SPEX	2160	A0
NGC 5005	05 Jun 2000	SPEX	720	A0V
NGC 5033	06 Jun 2000	SPEX	1200	A0V
NGC 5054	08 Jun 2000	SPEX	1200	A0V
NGC 5055	06 Jun 2000	SPEX	1200	A0V
NGC 5371	10 May 2001	CGS4	960	G5V
NGC 5566	06 Jun 2000	SPEX	720	A0V
NGC 5676	10 May 2001	CGS4	960	G5V
NGC 5713	10 May 2001	CGS4	960	G1V
NGC 5746	06 Apr 2001	SPEX	1560	A0V, G5
NGC 5846	05 Apr 2001	SPEX	1200	A0V, G5
NGC 5866	10 May 2001	CGS4	1200	G5V
NGC 5907	10 May 2001	CGS4	960	G5V
NGC 5985	10 May 2001	CGS4	960	G5V

Table 4. Spectral Features Identified in the Quiescent Composite K-Band Spectrum

Feature	Wavenumber (cm^{-1})	Wavelength (μm)
Mg I	4747	2.107
Mg I	4747	2.107
Al I	4740	2.110
Al I	4724	2.117
Na I	4533	2.206
Na I	4527	2.209
Fe I	4492	2.226
Fe I	4467	2.239
Ca I	4422	2.261
Ca I	4419	2.263
Ca I	4414	2.266
Mg I	4386	2.281
^{12}CO 2-0 bandhead	4360	2.294
^{12}CO 3-1 bandhead	4305	2.323
^{13}CO 2-0 bandhead	4265	2.345
^{12}CO 4-2 bandhead	4251	2.352
^{13}CO 3-1 bandhead	4212	2.374
^{12}CO 5-3 bandhead	4196	2.383

Table 5. Spectral Features Identified in the Quiescent Composite H-Band Spectrum

Feature	Wavenumber (cm^{-1})	Wavelength (μm)
^{12}CO 3-0 bandhead	6418	1.558
^{12}CO 4-1 bandhead	6337	1.578
Si I	6292	1.589
^{12}CO 5-2 bandhead	6257	1.598
^{12}CO 6-3 bandhead	6177	1.619
^{12}CO 7-4 bandhead	6097	1.640
^{12}CO 8-5 bandhead	6018	1.662
Al I	5977	1.673
Al I	5968	1.676
Al I	5964	1.677
^{12}CO 9-6 bandhead	5938	1.684
^{12}CO 10-7 bandhead	5959	1.707
Mg I	5843	1.711
^{12}CO 11-8 bandhead	5780	1.730

Table 6. Measurements of Absorption Line Features in the Composite Quiescent Spectra

Feature	Central Wavelength ^a (μm)	Equivalent Width (\AA)
Si I	1.5890	2.37 ± 0.05
CO 6-3	1.6198	3.55 ± 0.04
CO 2-0	2.2950	9.95 ± 0.03

^aAs defined by Origlia, Moorwood, & Oliva (1993)

Table 7. Measurement of Spectral Features in Non-Quiestcent Galaxies

Galaxy ^a	Fe II (1.6440 μm)		He I (2.0587 μm)		H ₂ 1-0 S(1) (2.1218 μm)		H I Br- γ (2.1661 μm)	
	Eq. Width (\AA)	Flux (W m^{-2})	Eq. Width (\AA)	Flux (W m^{-2})	Eq. Width (\AA)	Flux (W m^{-2})	Eq. Width (\AA)	Flux (W m^{-2})
NGC 289	2.2 ± 0.3	$1.6 \pm 0.2 \times 10^{-19}$	0.5 ± 0.2	$2.1 \pm 0.8 \times 10^{-20}$	3.8 ± 0.3	$1.6 \pm 0.1 \times 10^{-19}$	4.1 ± 0.3	$1.5 \pm 0.1 \times 10^{-19}$
NGC 1569 ^b	-0.4 ± 0.2	$-6.1 \pm 3.3 \times 10^{-19}$	1.7 ± 0.2	$4.4 \pm 0.6 \times 10^{-19}$	0.5 ± 0.2	$1.2 \pm 0.4 \times 10^{-19}$	1.3 ± 0.2	$2.8 \pm 0.3 \times 10^{-19}$
NGC 3556 ^c	15 ± 2	$6.8 \pm 0.8 \times 10^{-19}$	4 ± 2	$1.7 \pm 0.7 \times 10^{-19}$	28 ± 2	$1.20 \pm 0.07 \times 10^{-18}$
NGC 4088	-0.1 ± 0.4	$-0.2 \pm 1.2 \times 10^{-19}$	0.4 ± 0.4	$1.1 \pm 1.2 \times 10^{-19}$	2.8 ± 0.4	$7.2 \pm 1.1 \times 10^{-19}$
NGC 5005	4.8 ± 0.4	$8.8 \pm 0.7 \times 10^{-18}$	0.0 ± 0.2	$0.2 \pm 1.7 \times 10^{-19}$	10.4 ± 0.3	$8.0 \pm 0.3 \times 10^{-18}$	0.1 ± 0.8	$0.9 \pm 6.1 \times 10^{-19}$
NGC 5033	3.4 ± 0.3	$3.4 \pm 0.3 \times 10^{-18}$	0.3 ± 0.2	$1.3 \pm 0.8 \times 10^{-19}$	2.8 ± 0.2	$1.2 \pm 0.1 \times 10^{-18}$	1.9 ± 0.3	$7.8 \pm 1.1 \times 10^{-19}$
NGC 5676 ^d	23 ± 6	$4.0 \pm 1.1 \times 10^{-19}$	5 ± 8	$0.8 \pm 1.4 \times 10^{-19}$	70 ± 9	$1.1 \pm 0.1 \times 10^{-18}$
NGC 5713	7.1 ± 0.9	$1.7 \pm 0.2 \times 10^{-18}$	1.3 ± 0.9	$1.9 \pm 1.3 \times 10^{-19}$	2.8 ± 0.7	$3.8 \pm 0.9 \times 10^{-19}$	5.9 ± 1.3	$7.5 \pm 1.7 \times 10^{-19}$

^aThe nuclear region is used unless otherwise noted.

^bFor cluster A.

^cFor the west nuclear region.

^dFor the northern knot.

Table 8. Parameters Describing the Underlying Power Law Emission in NGC 5005 and NGC 5033

Galaxy	Spectral Index (α in $\lambda^{-\alpha}$)	Percent of K-band Flux
NGC 5005	1.7	7%
NGC 5033	1.7	22%

Table 9. Brackett- γ Luminosities and Luminosity-to-Mass Conversion Factors

Time Range (Myr)	Luminosity Range ^a (W)	Median Luminosity ^a (W)	Median Mass Remaining ^a (M_{\odot})	Luminosity-to-Mass Conversion Factor ($M_{\odot} W^{-1}$)
0.0 - 3.5	$3.1 \times 10^{31} - 9.0 \times 10^{31}$	8.6×10^{31}	9.9×10^5	1.2×10^{-26}
3.5 - 8.0	$6.5 \times 10^{29} - 3.0 \times 10^{31}$	3.9×10^{30}	9.4×10^5	2.4×10^{-25}

^aFor a burst that produces $10^6 M_{\odot}$ of stars.

Table 10. Fe II 1.644 μm Line Luminosities and Luminosity-to-Mass Conversion Factors

Time Range (Myr)	Supernova Rate Range ^a (yr ⁻¹)	Median Supernova Rate ^a (yr ⁻¹)	Median Luminosity ^a (W)	Median Mass Remaining ^a (M _⊙)	Luminosity-to-Mass Conversion Factor (M _⊙ W ⁻¹)
3.5 - 8.0	$7.7 \times 10^{-4} - 1.8 \times 10^{-3}$	8.8×10^{-4}	1.1×10^{31}	9.4×10^5	8.5×10^{-26}
8.0 - 36	$3.5 \times 10^{-4} - 7.6 \times 10^{-4}$	4.6×10^{-4}	5.5×10^{30}	8.3×10^5	1.5×10^{-25}

^aFor a burst that produces 10^6 M_⊙ of stars.

Table 11. Ratios of K-band Luminosities to Line Luminosities

Time Range (Myr)	K-Band Luminosity Range ^a (W)	Median K-Band Luminosity ^a (W)	K-Band / Brackett- γ Ratio	K-Band / Fe II Ratio
0.0 - 3.5	3.7×10^{32} - 6.1×10^{32}	5.8×10^{32}	6.7	...
3.5 - 8.0	2.9×10^{32} - 1.7×10^{33}	4.5×10^{32}	120	41
8.0 - 36	2.4×10^{32} - 2.3×10^{33}	3.1×10^{32}	...	56

^aFor a burst that produces $10^6 M_{\odot}$ of stars.

Table 12. Young and Old Stellar Masses and Their Ratios for Non-Quiescent Galaxies

Galaxy ^a	Age Range (Myr)	Spectral Line		Young Stellar Mass (M_{\odot})	Total System (W)	K Continuum			Old Stellar Mass (M_{\odot})	Young / Old Mass Ratio
		Name	Luminosity (W)			From Young Stars (W)	From Power-Law Continuum (W)	From Old Stars (W)		
NGC 289	3.5 - 8.0	Brackett- γ	6.8×10^{29}	1.6×10^5	6.8×10^{32}	8.2×10^{31}	...	6.0×10^{32}	7.8×10^6	2.1×10^{-2}
		Fe II	7.2×10^{29}	6.1×10^4	6.8×10^{32}	3.0×10^{31}	...	6.5×10^{32}	8.5×10^6	7.2×10^{-3}
NGC 1569 ^b	0.0 - 3.5	Brackett- γ	8.6×10^{27}	1.0×10^2	2.7×10^{31}	5.8×10^{28}	...	2.7×10^{31}	3.5×10^5	2.9×10^{-4}
NGC 3556 ^c	0.0 - 3.5	Brackett- γ	2.9×10^{30}	3.5×10^4	4.0×10^{32}	1.9×10^{31}	...	3.8×10^{32}	4.9×10^6	7.1×10^{-3}
NGC 4088	0.0 - 3.5	Brackett- γ	2.5×10^{30}	3.0×10^4	3.5×10^{33}	1.7×10^{31}	...	3.5×10^{33}	4.6×10^7	6.5×10^{-4}
NGC 5005	8.0 - 36	Fe II	4.8×10^{31}	7.2×10^6	1.6×10^{34}	2.7×10^{33}	1.1×10^{33}	1.2×10^{34}	1.6×10^8	4.5×10^{-2}
NGC 5033	8.0 - 36	Fe II	1.4×10^{31}	2.1×10^6	6.7×10^{33}	7.8×10^{32}	1.5×10^{33}	4.4×10^{33}	5.7×10^7	3.7×10^{-2}
NGC 5676 ^d	0.0 - 3.5	Brackett- γ	1.6×10^{31}	1.9×10^5	9.5×10^{32}	1.1×10^{32}	...	8.4×10^{32}	1.1×10^7	1.7×10^{-2}
NGC 5713	3.5 - 8.0	Brackett- γ	8.3×10^{30}	2.0×10^6	5.6×10^{33}	1.0×10^{33}	...	4.6×10^{33}	6.0×10^7	3.3×10^{-2}
		Fe II	1.9×10^{31}	1.6×10^6	5.6×10^{33}	7.8×10^{32}	...	4.8×10^{33}	6.2×10^7	2.6×10^{-2}

^aThe nuclear region is used unless otherwise noted.

^bFor cluster A.

^cFor the west nuclear region.

^dFor the northern knot.